

Construction of approximate entropy measure valued solutions for hyperbolic systems of conservation laws

Ulrik S. Fjordholm*, Roger Käppeli†, Siddhartha Mishra‡, Eitan Tadmor‡§

"There is no theory for the initial value problem for compressible flows in two space dimensions once shocks show up, much less in three space dimensions. This is a scientific scandal and a challenge."

P. D. Lax, 2007 Gibbs Lecture [46]

Abstract

Numerical evidence is presented to demonstrate that state of the art numerical schemes need not converge to entropy solutions of systems of hyperbolic conservation laws in several space dimensions. Combined with recent results on the lack of stability of these solutions, we advocate the more general notion of entropy measure valued solutions as the appropriate paradigm for solutions of such multi-dimensional systems.

We propose a detailed numerical procedure which constructs approximate entropy measure valued solutions, and we prove sufficient criteria that ensure their (narrow) convergence, thus providing a viable numerical framework for the approximation of entropy measure valued solutions. Examples of schemes satisfying these criteria are presented. A number of numerical experiments, illustrating our proposed procedure and examining interesting properties of the entropy measure valued solutions, are also provided.

1991 Mathematics Subject Classification. 65M06, 35L65, 35R06.

Keywords and phrases. Hyperbolic conservation laws, uniqueness, stability, entropy condition, measure-valued solutions, atomic initial data, random field, weak BV estimate, narrow convergence.

*Department of Mathematical Sciences, Norwegian University of Science and Technology, Trondheim, N-7491, Norway

†Seminar for Applied Mathematics, ETH Zürich, Rämistrasse 101, Zürich, Switzerland

‡Department of Mathematics, Center of Scientific Computation and Mathematical Modeling (CSCAMM), Institute for Physical sciences and Technology (IPST), University of Maryland MD 20742-4015, USA

§S.M. was supported in part by ERC STG. N 306279, SPARCCL. E.T. was supported in part by NSF grants DMS10-08397, RNMS11-07444 (KI-Net) and ONR grant N00014-1210318. Many of the computations were performed at CSCS Lugano through Project s345. SM thanks Prof. Christoph Schwab (ETH Zurich) for several helpful comments and suggestions.

Contents

1	Introduction	3
1.1	Mathematical framework	3
1.2	Numerical schemes	4
1.3	Two numerical experiments	5
1.4	A different notion of solutions	7
1.5	Aims and scope of the current paper	8
2	Young measures and entropy measure valued solutions	9
2.1	The measure valued (MV) Cauchy problem	10
3	Well-posedness of EMV solutions	11
3.1	Scalar conservation laws	11
3.2	Systems of conservation laws	14
4	Construction of approximate EMV solutions	16
4.1	Numerical approximation of EMV solutions	16
4.2	What are we computing – narrow convergence of space-time averages	22
5	Examples of narrowly convergent numerical schemes	24
5.1	Scalar conservation laws	24
5.2	Systems of conservation laws	25
6	Numerical Results	26
6.1	Kelvin-Helmholtz problem: mesh refinement ($\Delta x \downarrow 0$)	27
6.2	Kelvin-Helmholtz: vanishing variance around atomic initial data ($\varepsilon \downarrow 0$)	31
6.3	Richtmeyer-Meshkov problem	37
6.4	Measure valued (MV) stability	41
7	Discussion	46
A	Young measures	51
A.1	Probability measures	51
A.2	Young measures	53
A.3	Random fields and Young measures	55
B	Proof of Theorem 4.9	57
C	Time continuity of approximations	59

1 Introduction

A large number of problems in physics and engineering are modeled by systems of conservation laws

$$\partial_t u + \nabla_x \cdot f(u) = 0 \quad (1.1a)$$

$$u(x, 0) = u_0(x). \quad (1.1b)$$

Here, the unknown $u = u(x, t) : \mathbb{R}^d \times \mathbb{R}_+ \rightarrow \mathbb{R}^N$ is the vector of conserved variables and $f = (f^1, \dots, f^d) : \mathbb{R}^N \rightarrow \mathbb{R}^{N \times d}$ is the flux function. We denote $\mathbb{R}_+ := [0, \infty)$.

The system (1.1a) is hyperbolic if the flux Jacobian $\partial_u(f \cdot n)$ has real eigenvalues for all $n \in \mathbb{R}^d$ with $|n| = 1$. Examples for hyperbolic systems of conservation laws include the shallow water equations of oceanography, the Euler equations of gas dynamics, the magnetohydrodynamics (MHD) equations of plasma physics, the equations of nonlinear elastodynamics and the Einstein equations of cosmology. We refer to [17, 35] for more theory on hyperbolic conservation laws.

1.1 Mathematical framework

It is well known that solutions of the Cauchy problem (1.1) can develop discontinuities such as shock waves in finite time, even when the initial data is smooth. Hence, solutions of hyperbolic systems of conservation laws (1.1) are sought in the weak (distributional) sense.

Definition 1.1. A function $u \in L^\infty(\mathbb{R}^d \times \mathbb{R}_+, \mathbb{R}^N)$ is a weak solution of (1.1) if it satisfies (1.1) in the sense of distributions:

$$\int_{\mathbb{R}_+} \int_{\mathbb{R}^d} \partial_t \varphi(x, t) u(x, t) + \nabla_x \varphi(x, t) \cdot f(u(x, t)) \, dx dt + \int_{\mathbb{R}^d} \varphi(x, 0) u_0(x) \, dx = 0 \quad (1.2)$$

for all test functions $\varphi \in C_c^1(\mathbb{R}^d \times \mathbb{R}_+)$.

Weak solutions are in general not unique: infinitely many weak solutions may exist after the formation of discontinuities. Thus, to obtain uniqueness, additional admissibility criteria have to be imposed. These admissibility criteria take the form of entropy conditions, which are formulated in terms of entropy pairs.

Definition 1.2. A pair of functions (η, q) with $\eta : \mathbb{R}^N \rightarrow \mathbb{R}$, $q : \mathbb{R}^N \rightarrow \mathbb{R}^d$ is called an entropy pair if η is convex and q satisfies the compatibility condition $q' = \eta' \cdot f'$.

Definition 1.3. A weak solution u of (1.1) is an entropy solution if the entropy inequality

$$\partial_t \eta(u) + \nabla_x \cdot q(u) \leq 0 \quad \text{in } \mathcal{D}'(\mathbb{R}^d \times \mathbb{R}_+)$$

is satisfied for all entropy pairs (η, q) , that is, if

$$\int_{\mathbb{R}_+} \int_{\mathbb{R}^d} \partial_t \varphi(x, t) \eta(u(x, t)) + \nabla_x \varphi(x, t) \cdot q(u(x, t)) \, dx dt + \int_{\mathbb{R}^d} \varphi(x, 0) \eta(u_0(x)) \, dx \geq 0 \quad (1.3)$$

for all nonnegative test functions $0 \leq \varphi \in C_c^1(\mathbb{R}^d \times \mathbb{R}_+)$.

For the special case of scalar conservation laws ($N = 1$), every convex function η gives rise to an entropy pair by letting $q(u) := \int^u \eta'(\xi) f'(\xi) d\xi$. This rich family of entropy pairs was used by Kruzhkov [43] to obtain existence, uniqueness and stability of solutions for scalar conservation laws.

Corresponding (global) well-posedness results for systems of conservation laws are much harder to obtain. Lax [45] showed existence and stability of entropy solutions for one-dimensional systems of conservation laws for the special case of Riemann initial data. Existence results for the Cauchy problem for one-dimensional systems were obtained by Glimm in [33] using the random choice method and by Bianchini and Bressan [6] with the vanishing viscosity method. Uniqueness and stability results for one-dimensional systems were shown by Bressan and co-workers [10]. All of these results rely on an assumption that the initial data is “sufficiently small”, i.e., lies sufficiently close to some constant.

On the other hand, no global existence and uniqueness (stability) results are currently available for a generic system of conservation laws in several space dimensions. In fact, recent results (see [18, 19] and references therein) provide counterexamples which illustrate that entropy weak solutions for multi-dimensional systems of conservation laws are not necessarily unique.

1.2 Numerical schemes

Numerical schemes have played a leading role in the study of systems of conservation laws. A wide variety of numerical methods for approximating (1.1) are currently available. These include the very popular and highly successful numerical framework of finite volume (difference) schemes, based on approximate Riemann solvers or on Riemann-solver-free centered differencing, [35, 14, 48, 11], which utilize TVD [36], ENO [37] or WENO [40] non-oscillatory reconstruction techniques and strong stability preserving (SSP) Runge-Kutta time integrators [32]. Another popular alternative is the Discontinuous Galerkin finite element method [15].

The goal in the analysis of numerical schemes approximating (1.1) is proving convergence to an entropy solution as the mesh is refined. This issue has been addressed in the special case of (first-order) monotone schemes for scalar conservation laws (see [16] for the one-dimensional case and [13] for multiple dimensions) using the TVD property. Corresponding convergence results for arbitrarily (formally) high-order finite difference schemes for scalar conservation laws was obtained recently in [26], see also [25]. Convergence results for (arbitrarily high order) space time DG discretization for scalar conservation laws were obtained in [39] and for the spectral viscosity method in [61].

The question of convergence of numerical schemes for systems of conservation laws is significantly harder. Currently, there are no rigorous proofs of convergence for any kind of finite volume (difference) and finite element methods to the entropy solutions of a generic system of conservation laws, even in one space dimension. Convergence aside, even the stability of numerical approximations to systems of conservation laws is mostly open. The only notion of numerical stability for systems of conservation laws that has been analyzed rigorously so far is that of entropy stability – the design of numerical approximations that satisfy a discrete version of the entropy inequality. Such schemes have been devised in [59, 60, 25, 38]. However, entropy stability may not suffice to ensure the convergence of approximate solutions.

1.3 Two numerical experiments

Given the lack of rigorous stability and convergence results for systems of conservation laws, it has become customary in the field to rely on benchmark numerical tests to demonstrate the convergence of the scheme empirically. One such benchmark test case is the radial Sod shock tube [48].

1.3.1 Sod shock tube

In this test, we consider the compressible Euler equations of gas dynamics in two space dimensions (see Section 6) as a prototypical hyperbolic system of conservation laws. The initial data for the two-dimensional version of the well-known Sod shock tube problem is given by

$$u_0(x) = \begin{cases} u_L & \text{if } |x| \leq r_0 \\ u_R & \text{if } |x| > r_0, \end{cases} \quad (1.4)$$

with $\rho_L = p_L = 3$, $\rho_R = p_R = 1$, $w^x = w^y = 0$.

To begin with, we consider a perturbed version of the Sod shock tube by setting the initial data

$$u_0^\varepsilon(x) = u_0(x) + \varepsilon X, \quad (1.5)$$

where $\varepsilon > 0$ is a small number. The perturbation X is set as

$$X_\rho = X_p = 0, \quad X_{w^x}(x) = \sin(2\pi x_1), \quad X_{w^y}(x) = \sin(2\pi x_2). \quad (1.6)$$

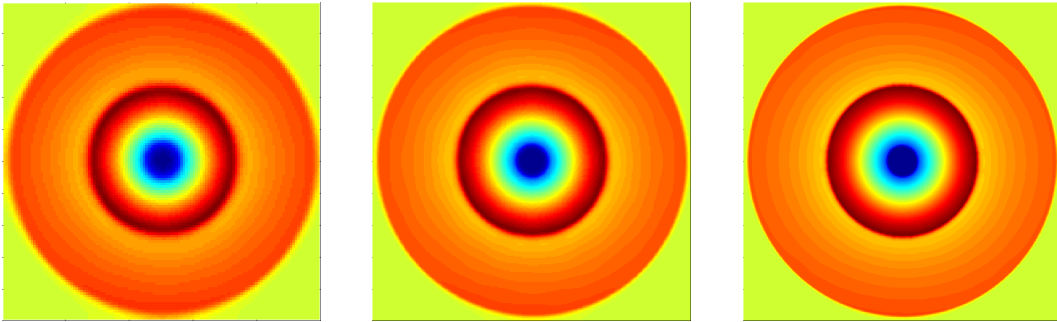


Figure 1.1: Density for the Sod shock tube problem, computed with TECNO2 finite difference scheme of [25], with initial data (1.5) at time $t = 0.24$. Left to right: $\Delta x = 1/128, 1/256, 1/512$.

First we set $\varepsilon = 0.01$ and compute the approximate solutions of the two-dimensional Euler equations (6.1) with the second-order TeCNO2 finite difference scheme of [25]. In Figure 1.1, we present the computed densities at time $t = 0.24$ for different mesh resolutions. The figure clearly indicates convergence as the mesh is refined. To further quantify this convergence, we compute the difference in the approximate solution on two successive mesh resolutions:

$$E^{\Delta x} = \|u^{\Delta x} - u^{\Delta x/2}\|_{L^1([0,1]^2)}, \quad (1.7)$$

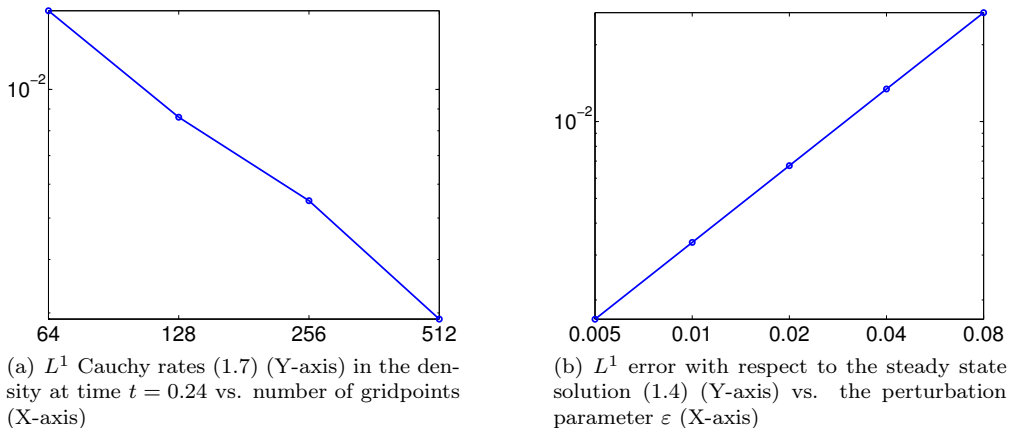


Figure 1.2: L^1 differences in density ρ at time $t = 0.24$ for the Sod shock tube problem with initial data (1.5).

and plot the results for density in Figure 1.2(a). The results clearly show that the numerical approximations, form a Cauchy sequence in L^1 , and hence converge. The same numerical experiment was performed with a different scheme: a second-order high-resolution scheme based on an HLLC solver using the MC limiter, implemented in the FISH code [42]. Similar convergence results were obtained (omitted here for brevity).

Next, we investigate numerically the issue of stability of this system with respect to perturbations in the initial data. To this end, we let the perturbation amplitude $\varepsilon \rightarrow 0$ in (1.5) and plot the error in computed density (at a fixed mesh resolution of 1024^2 points) and the exact solution (of the unperturbed initial data (1.4)), for successively lower values of ε in Figure 1.2(b). The results clearly show convergence to the unperturbed solution in the zero ε limit.

The above numerical example suggests that one might expect convergence of the approximate numerical solutions to the entropy solution. The computed solutions were observed to be stable with respect to initial data. In the literature it is common to extrapolate from benchmark test cases like the Sod shock tube and expect that the underlying numerical approximations converge as the mesh is refined.

1.3.2 Kelvin-Helmholtz problem

We question the universality of the above empirical convergence and stability results by considering the following set of initial data for the two-dimensional Euler equations (see Section 6):

$$u_0(x) = \begin{cases} u_L & \text{if } 0.25 < x_2 < 0.75 \\ u_R & \text{if } x_2 \leq 0.25 \text{ or } x_2 \geq 0.75, \end{cases} \quad (1.8)$$

with $\rho_L = 2$, $\rho_R = 1$, $w_L^x = -0.5$, $w_R^x = 0.5$, $w_L^y = w_R^y = 0$ and $p_L = p_R = 2.5$. It is readily seen that this is a steady state, i.e., that $u(x, t) \equiv u_0(x)$ is an entropy solution.

Next, we add the same perturbation (1.5) to the initial data (1.8) and compute approximate solutions for different $\Delta x > 0$. A series of approximate solutions using perturbation amplitude $\varepsilon = 0.01$ are shown in Figure 1.3. The results show that there is no sign of any convergence as the mesh is refined. As a matter of fact, structures at smaller and smaller scales are formed with mesh refinement. This lack of convergence is quantified by plotting the differences between successive mesh levels (1.7) for the density in Figure 1.4(a). The results show that as the mesh is refined, the approximate solutions do not form a Cauchy sequence in L^1 , and hence do not converge. The results presented in Figures 1.3 and (1.4)(a) are with the TeCNO scheme of [25]. Very similar results were also obtained with the FISH code [42] and the ALSVID finite volume code [29]. Furthermore, convergence in even weaker $W^{-1,p}$, $1 < p \leq \infty$, norms was also not observed. Thus, one cannot deduce convergence of even bulk properties of the flow, such as the average domain temperature, in this particular case.

Finally, we check stability of the numerical solutions as the perturbation parameter $\varepsilon \rightarrow 0$. We compute numerical approximations at a fixed fine grid resolution of 1024^2 points with successively lower values of ε . These results are compared with the steady state solution (1.8) in Figure presented in Figure 1.4(b). The L^1 difference results clearly show that there is no convergence to the steady state solution (1.8) as $\varepsilon \rightarrow 0$.

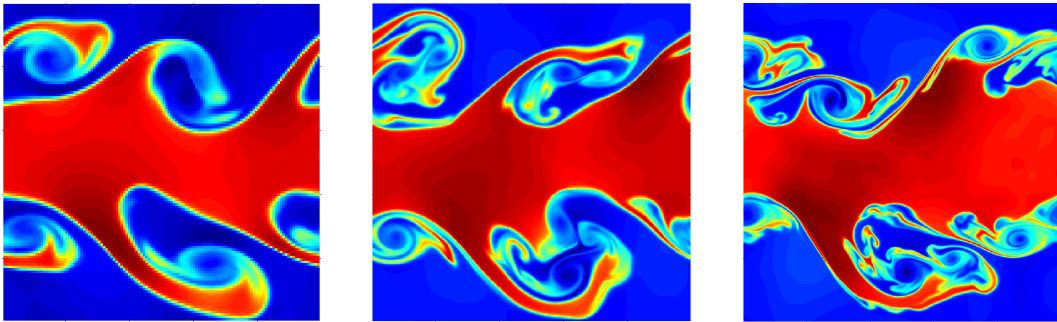


Figure 1.3: Density for the Kelvin-Helmholtz problem (1.8) with perturbation (1.5) and perturbation parameter $\varepsilon = 0.01$. Left to right: $\Delta x = 1/128, 1/256, 1/512$, at time $t = 1$

1.4 A different notion of solutions

Contrary to the widely accepted notion that state of the art numerical schemes converge to an entropy solution of (1.1) under mesh refinement, the above numerical example clearly demonstrates that*

- Standard numerical schemes (finite volume, finite difference, DG) may not converge to any function as the mesh is refined. In particular, new structures are found at smaller and smaller scales as the mesh is refined.

*We have tested at least three types of schemes, TeCNO scheme of [25], the high-resolution HLLC scheme of [42] and the finite volume scheme of [29], and obtained similar non-convergence and instability results as presented above. We strongly suspect that any numerical method will not converge or be stable with respect to perturbations in the initial data for this particular example.

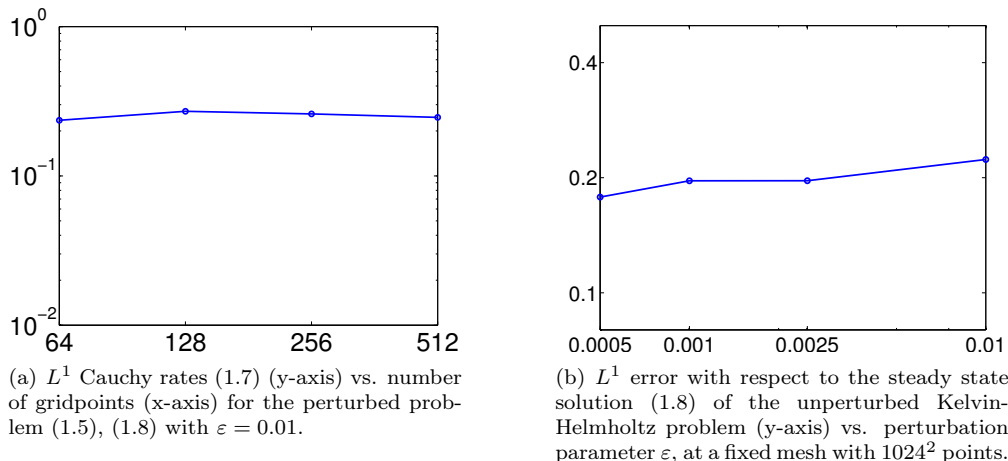


Figure 1.4: L^1 differences in density ρ at time $t = 2$ for the Kelvin-Helmholtz problem (1.8).

- Entropy solutions (and their numerical approximations) may not be L^p -stable (for any $p \geq 1$) with respect to perturbations of the initial data.

The above discussion strongly suggests that the standard notion of entropy solutions for (multi-dimensional) systems of conservation laws is not adequate in many respects. In particular, entropy solutions may not suffice to characterize the limits of numerical approximations to conservation laws in a stable manner. Taken together with the recent counterexamples to stability in [18, 19], we postulate the need to seek a different (more general) notion of solutions to systems of conservation laws. Entropy solutions (whenever they exist) should be included within this class of solutions.

Based on the fact that oscillations persist on finer and finer scales (see Figure 1.3) for numerical approximations of (1.1), we focus on the concept of entropy measure valued solutions, introduced by DiPerna in [22], see also [23]. In this framework, solutions of the system of conservation laws (1.1) are no longer integrable functions, but parameterized probability measures or Young measures, which are able to represent the limit behavior of sequences of oscillatory functions. This solution concept was further based on the work of Tartar [62] on characterizing the weak limits of bounded sequences of functions. More recently, Glimm and co-workers ([12, 49] and references therein) have also hypothesized that entropy measure valued solutions are the appropriate notion of solutions for hyperbolic conservation laws, particularly in several space dimensions.

1.5 Aims and scope of the current paper

In the current paper:

- We replace the Cauchy problem (1.1) with a more general initial value problem where the initial data is a Young measure. The resulting solutions are interpreted as entropy

measure valued solutions, in the sense of DiPerna [22]. We study the existence and stability of the entropy measure valued solutions.

- The main aim of the current paper is to approximate the entropy measure valued solutions numerically. To this end, we propose an algorithm based on the realization of Young measures as the law of random fields and approximate the solution random fields with suitable finite difference numerical schemes. We propose a set of sufficient conditions that a scheme has to satisfy in order to converge to an entropy measure valued solution as the mesh is refined. Examples of such convergent schemes are also provided.
- We present a large number of numerical experiments to validate the proposed theory. The numerical approximations are also employed to study the stability as well as other interesting properties of entropy measure valued solutions.

The rest of this paper is organized as follows: in Section 2, we provide a short but self-contained description of Young measures (see also Appendix A) and then define entropy measure valued solutions for a generalized Cauchy problem, corresponding to the system of conservation law (1.1). The well-posedness of the entropy measure valued solutions is discussed in Section 3. In Section 4, we discuss finite difference schemes approximating (1.1) and propose abstract criteria that these schemes have to satisfy in order to converge to entropy measure valued solutions. Two schemes satisfying the abstract convergence framework are presented in Section 5. In Section 6, we present numerical experiments that illustrate the convergence properties of the schemes and discuss the stability and related properties of entropy measure valued solutions.

2 Young measures and entropy measure valued solutions

A Young measure on a set $D \subset \mathbb{R}^k$ is a function ν which assigns to every point $y \in D$ a probability measure $\nu_y \in \mathcal{P}(\mathbb{R}^N)$ on the phase space \mathbb{R}^N . The set of all Young measures from D to \mathbb{R}^N is denoted by $\mathbf{Y}(D, \mathbb{R}^N)$. We can compose a Young measure with a continuous function g by defining $\langle \nu_y, g \rangle := \int_{\mathbb{R}^N} g(\xi) d\nu_y(\xi)$, the expectation of g with respect to the probability measure ν_y . Note that this defines a real-valued function of $y \in D$.

Every measurable function $u : D \rightarrow \mathbb{R}^N$ gives rise to a Young measure by letting

$$\nu_y := \delta_{u(y)},$$

where δ_ξ is the Dirac measure centered at $\xi \in \mathbb{R}^N$. Such Young measures are called atomic.

If ν^1, ν^2, \dots is a sequence of Young measures then there are two notions of convergence. Following [2], we say that ν^n converge narrowly to a Young measure ν (written $\nu^n \rightharpoonup \nu$) if $\langle \nu^n, g \rangle \xrightarrow{*} \langle \nu, g \rangle$ in $L^\infty(D)$ for all $g \in C_0(\mathbb{R}^N)$, that is, if

$$\int_D \varphi(z) \langle \nu_z^n, g \rangle dz \rightarrow \int_D \varphi(z) \langle \nu_z, g \rangle dz \quad \forall \varphi \in L^1(D). \quad (2.1)$$

By the fundamental theorem of Young measures (see Theorem A.1), any suitably bounded sequence of Young measures has a narrowly convergent subsequence.

We say that the sequence $\{\nu^n\}$ converges strongly to ν (written $\nu^n \rightarrow \nu$) if

$$\|W_p(\nu^n, \nu)\|_{L^p(D)} \rightarrow 0 \quad (2.2)$$

for some $p \in [1, \infty)$, where W_p is the p -Wasserstein distance

$$W_p(\mu, \rho) := \inf \left\{ \int_{\mathbb{R}^N \times \mathbb{R}^N} |\xi - \zeta|^p d\pi(\xi, \zeta) : \pi \in \Pi(\mu, \rho) \right\}^{1/p}$$

which metricizes the topology of narrow convergence on the set $\mathcal{P}^p(\mathbb{R}^N) := \{\mu \in \mathcal{P}(\mathbb{R}^N) : \langle \nu, |\xi|^p \rangle < \infty\}$. Here, $\Pi(\mu, \rho)$ is the set of probability measures on $\mathbb{R}^N \times \mathbb{R}^N$ with marginals $\mu, \rho \in \mathcal{P}^p(\mathbb{R}^N)$ (see also Appendix A.1.3).

We refer to Appendix A for a more rigorous and detailed introduction to Young measures.

2.1 The measure valued (MV) Cauchy problem

As mentioned in the introduction, we will seek a more general (weaker) notion of solutions to the Cauchy problem for a systems of conservation laws (1.1) by requiring that the solutions be Young measures, instead of integrable functions. Equipped with the notation of the previous section, we propose the following generalized Cauchy problem (corresponding to the system (1.1))

$$\begin{aligned} \partial_t \langle \nu, \text{id} \rangle + \nabla_x \cdot \langle \nu, f \rangle &= 0 \\ \nu_{(x,0)} &= \sigma_x, \end{aligned} \quad (2.3)$$

where $\sigma \in \mathbf{Y}(\mathbb{R}^d, \mathbb{R}^N)$ is the initial measure-valued data.

The solutions to the above MV Cauchy problem are defined as follows.

Definition 2.1. A Young measure $\nu \in \mathbf{Y}(\mathbb{R}^d \times \mathbb{R}_+, \mathbb{R}^N)$ is a measure-valued (MV) solution of (2.3) if (2.3) holds in the sense of distributions, i.e.,

$$\int_{\mathbb{R}_+} \int_{\mathbb{R}^d} \partial_t \varphi(x, t) \langle \nu_{(x,t)}, \text{id} \rangle + \nabla_x \varphi(x, t) \cdot \langle \nu_{(x,t)}, f \rangle dx dt + \int_{\mathbb{R}^d} \varphi(x, 0) \langle \sigma_x, \text{id} \rangle dx = 0 \quad (2.4)$$

for all test functions $\varphi \in C_c^1(\mathbb{R}^d \times \mathbb{R}_+)$.

Definition 2.2. A Young measure $\nu \in \mathbf{Y}(\mathbb{R}^d \times \mathbb{R}_+, \mathbb{R}^N)$ is an entropy measure-valued (EMV) solution of (2.3) if in addition to being a measure valued solution (satisfying (2.4)), it also satisfies,

$$\partial_t \langle \nu, \eta \rangle + \nabla_x \cdot \langle \nu, q \rangle \leq 0 \quad \text{in } \mathcal{D}'(\mathbb{R}^d \times \mathbb{R}_+) \quad (2.5)$$

for every entropy pair (η, q) , that is, if

$$\int_{\mathbb{R}_+} \int_{\mathbb{R}^d} \partial_t \varphi(x, t) \langle \nu_{(x,t)}, \eta \rangle + \nabla_x \varphi(x, t) \cdot \langle \nu_{(x,t)}, q \rangle dx dt + \int_{\mathbb{R}^d} \varphi(x, 0) \langle \sigma_x, \eta \rangle dx \geq 0 \quad (2.6)$$

for all nonnegative test functions $0 \leq \varphi \in C_c^1(\mathbb{R}^d \times \mathbb{R}_+)$.

We denote by $\mathcal{E}(\sigma)$ the set of all entropy MV solutions of the MV Cauchy problem (2.3) with initial MV data σ . It is readily seen that every entropy solution u of (1.1) gives rise to an EMV solution of (2.3) by defining $\nu_{(x,t)} := \delta_{u(x,t)}$, the atomic Young measure concentrated at u . Thus, the set $\mathcal{E}(\sigma)$ is at least as large as the set of entropy solutions of (1.1) whenever σ is atomic, $\sigma = \delta_{u_0}$.

Remark 2.3. It is to be noted that the notion of entropy measure valued solutions of DiPerna [22], focuses on the MV Cauchy problem (2.3) with atomic initial data i.e, $\sigma_x = \delta_{u_0(x)}$ for some measurable $u_0 : \mathbb{R}^d \mapsto \mathbb{R}^N$.

Remark 2.4. In practice, the initial data u_0 in (1.1a) is obtained from a measurement or observation process. Since measurements (observations) are intrinsically uncertain, it is customary to model this initial uncertainty statistically by considering the initial data u_0 as a random field. Given the fact that the law of a random field is a Young measure, we can also model this initial uncertainty with non-atomic initial measures in the measure valued (MV) Cauchy problem (2.3). Thus, our formulation also includes various formalisms for uncertainty quantification of conservation laws, i.e., the determination of solution uncertainty given uncertain initial data. See [51, 52, 53] and references therein, for an extensive discussion on uncertainty quantification for conservation laws.

3 Well-posedness of EMV solutions

The questions of existence, uniqueness and stability of EMV solutions of (2.3) are of fundamental significance. We start with the scalar case.

3.1 Scalar conservation laws

The question of existence of EMV solutions for scalar conservation laws was considered by DiPerna in [22]. We generalize his result for a non-atomic initial data as follows.

Theorem 3.1. Consider the MV Cauchy problem (2.3) for a scalar conservation law. If the initial data σ is uniformly bounded (see Appendix A.2.2), then there exists an EMV solution of (2.3).

Proof. By Proposition A.3, there exists a probability space (Ω, \mathcal{F}, P) and a random field $u_0 : \Omega \times \mathbb{R}^d \rightarrow \mathbb{R}$ with law σ . By the uniform boundedness of σ , we have $\|u_0\|_{L^\infty(\Omega \times \mathbb{R}^d)} < \infty$.

For each $\omega \in \Omega$, let $u(\omega; x, t)$ be the entropy solution of (1.1) with initial data $u_0(\omega)$, and define ν as the law of u . Then for every entropy pair (η, q) and every test function

$0 \leq \varphi \in C_c^1(\mathbb{R}^d \times [0, \infty))$, we have

$$\begin{aligned}
& \int_{\mathbb{R}_+} \int_{\mathbb{R}^d} \partial_t \varphi(x, t) \langle \nu_{(x, t)}, \eta \rangle + \nabla_x \varphi(x, t) \cdot \langle \nu_{(x, t)}, q \rangle \, dx dt \\
&= \int_{\mathbb{R}_+} \int_{\mathbb{R}^d} \partial_t \varphi(x, t) \int_{\Omega} \eta(u(\omega; x, t)) \, dP(\omega) + \nabla_x \varphi(x, t) \cdot \int_{\Omega} q(u(\omega; x, t)) \, dP(\omega) \, dx dt \\
&= \int_{\Omega} \int_{\mathbb{R}_+} \int_{\mathbb{R}^d} \partial_t \varphi(x, t) \eta(u(\omega; x, t)) + \nabla_x \varphi(x, t) \cdot q(u(\omega; x, t)) \, dx dt dP(\omega) \\
&\geq - \int_{\Omega} \int_{\mathbb{R}^d} \varphi(x, 0) \eta(u_0(\omega; x)) \, dx dP(\omega) \\
&= - \int_{\mathbb{R}^d} \varphi(x, 0) \langle \sigma_x, \eta \rangle \, dx,
\end{aligned}$$

by Fubini's theorem and the entropy stability of $u(\omega)$ for each ω . This proves the entropy inequality (2.6). \square

Although EMV solutions exist for scalar conservation laws, they may not be unique (see Schochet [57]). Here is a simple counter-example.

Example 3.2. Consider Burgers' equation

$$\partial_t u + \partial_x \left(\frac{u^2}{2} \right) = 0.$$

Denote by λ the Lebesgue measure on \mathbb{R} . We define $\Omega = [0, 1]$, $\mathcal{F} = \mathcal{B}([0, 1])$ and $P = \lambda_{[0, 1]}$, where λ_A is the restriction of λ to the set A , $\lambda_A(B) = \lambda(A \cap B)$. Let u_0 and \tilde{u}_0 be the random variables

$$u_0(\omega; x) := \begin{cases} 1 + \omega & \text{for } x < 0 \\ \omega & \text{for } x > 0, \end{cases} \quad \tilde{u}_0(\omega; x) := \begin{cases} 1 + \omega & \text{for } x < 0 \\ 1 - \omega & \text{for } x > 0, \end{cases} \quad \omega \in [0, 1], \, x \in \mathbb{R}.$$

It is readily checked that the law of both u_0 and \tilde{u}_0 in (Ω, \mathcal{F}, P) is

$$\sigma_x = \begin{cases} \lambda_{[1, 2]} & \text{for } x < 0 \\ \lambda_{[0, 1]} & \text{for } x > 0. \end{cases}$$

The entropy solutions $u(\omega)$ and $\tilde{u}(\omega)$ of the Riemann problems with initial data $u_0(\omega)$ and $\tilde{u}_0(\omega)$ are given by

$$u(\omega; x, t) = \begin{cases} 1 + \omega & \text{if } x/t < 1/2 + \omega \\ \omega & \text{if } x/t > 1/2 + \omega; \end{cases} \quad \tilde{u}(\omega; x, t) = \begin{cases} 1 + \omega & \text{if } x/t < 1 \\ 1 - \omega & \text{if } x/t > 1. \end{cases}$$

To compute the law ν of u we rewrite u as

$$u(\omega; x, t) = \begin{cases} 1 + \omega & \text{if } x/t - 1/2 < \omega \\ \omega & \text{if } x/t - 1/2 > \omega. \end{cases}$$

Hence, if $x/t - 1/2 < 0$ then $\nu_{(x,t)} = \lambda_{[1,2]}$, whereas if $x/t - 1/2 > 1$ then $\nu_{(x,t)} = \lambda_{[0,1]}$. When $0 \leq x/t - 1/2 \leq 1$ we have for every $g \in C_0(\mathbb{R}^N)$

$$\begin{aligned} \langle \nu_{(x,t)}, g \rangle &= \int_0^1 g(u(\omega; x, t)) \, d\omega = \int_{x/t-1/2}^1 g(1+\omega) \, d\omega + \int_0^{x/t-1/2} g(\omega) \, d\omega \\ &= \int_{x/t+1/2}^2 g(\omega) \, d\omega + \int_0^{x/t-1/2} g(\omega) \, d\omega = \int_{\mathbb{R}} g(\omega) \, d\lambda_{[x/t+1/2, 2]}(\omega) + \int_{\mathbb{R}} g(\omega) \, d\lambda_{[0, x/t-1/2]}(\omega). \end{aligned}$$

After a similar calculation for $\tilde{\nu}$ we find that

$$\nu_{(x,t)} = \begin{cases} \lambda_{[1,2]} & \text{if } x/t < 1/2 \\ \lambda_{[x/t+1/2, 2]} + \lambda_{[0, x/t-1/2]} & \text{if } 1/2 < x/t < 3/2 \\ \lambda_{[0,1]} & \text{if } 3/2 < x/t, \end{cases} \quad \tilde{\nu}_{(x,t)} = \begin{cases} \lambda_{[1,2]} & \text{if } x/t < 1 \\ \lambda_{[0,1]} & \text{if } x/t > 1. \end{cases}$$

Thus, ν and $\tilde{\nu}$ are EMV solutions with the same initial MV data σ , but do not coincide.

The non-uniqueness of EMV solutions, already at the level of scalar conservation laws, raises serious questions whether the notion of an entropy measure-valued solution is useful. However, the following result shows that when restricting attention to the relevant class of atomic initial data, then EMV solutions of the scalar MV Cauchy problem (2.3) are stable.

Theorem 3.3. Consider the scalar case $N = 1$. Let $u_0 \in L^\infty(\mathbb{R}^d)$ and let $\sigma \in \mathbf{Y}(\mathbb{R}^d)$ be uniformly bounded. Let $u \in L^\infty(\mathbb{R}^d \times \mathbb{R}_+)$ be the entropy solution of the scalar conservation law (1.1) with initial data u_0 . Let ν be any EMV solution of (2.3) which attains the initial MV data σ in the sense

$$\lim_{T \rightarrow 0} \frac{1}{T} \int_0^T \int_{\mathbb{R}^d} \langle \nu_{(x,t)}, |u_0(x) - \xi| \rangle \, dx dt = 0.$$

Then for all $t > 0$,

$$\int_{\mathbb{R}^d} \langle \nu_{(x,t)}, |u(x,t) - \xi| \rangle \, dx \leq \int_{\mathbb{R}^d} \langle \sigma_x, |u_0(x) - \xi| \rangle \, dx,$$

or equivalently,

$$\left\| W_1(\nu_{(\cdot, t)}, \delta_{u(\cdot, t)}) \right\|_{L^1(\mathbb{R}^d)} \leq \left\| W_1(\sigma, \delta_{u_0}) \right\|_{L^1(\mathbb{R}^d)}.$$

In particular, if $\sigma = \delta_{u_0}$ then $\nu = \delta_u$.

Proof. We follow DiPerna [22] who proved the uniqueness of scalar MV solutions subject to atomic initial data. Here, we quantify stability in terms of the W_1 -metric, which is related to the $L^1(x, v)$ -stability of kinetic solutions associated with (1.1); see [56].

For $\xi \in \mathbb{R}$, let $(\eta(\xi, u), q(\xi, u))$ be the Kruzkov entropy pair, defined as

$$\eta(\xi, u) := |\xi - u|, \quad q(\xi, u) := \operatorname{sgn}(\xi - u)(f(\xi) - f(u)).$$

By [22, Theorem 4.1] we know that for any entropy solution u of (1.1) and any entropy MV solution ν of (2.3), we have

$$\partial_t \langle \nu_z, \eta(\xi, u(z)) \rangle + \nabla_x \cdot \langle \nu_z, q(\xi, u(z)) \rangle \leq 0 \quad \text{in } \mathcal{D}'(\mathbb{R}^d \times (0, \infty)),$$

that is,

$$\int_{\mathbb{R}_+} \int_{\mathbb{R}^d} \left(\partial_t \varphi(x, t) \int_{\mathbb{R}^N} \eta(\xi, u(x, t)) d\nu_{(x,t)}(\xi) + \nabla_x \varphi(x, t) \cdot \int_{\mathbb{R}^N} q(\xi, u(x, t)) d\nu_{(x,t)}(\xi) \right) dx dt \geq 0$$

for all test functions $0 \leq \varphi \in C_c^1(\mathbb{R}^d \times (0, \infty))$. In particular the function

$$V(t) := \int_{\mathbb{R}^d} \langle \nu_{(x,t)}, |\xi - u(x, t)| \rangle dx$$

is nonincreasing. By hypothesis, the point $t = 0$ is a Lebesgue point for V , so $\lim_{t \rightarrow 0} V(t) = \int_{\mathbb{R}^d} \langle \sigma_x, |u_0(x) - \xi| \rangle dx$. The result follows. \square

3.2 Systems of conservation laws

It is clear from the above discussion that non-atomic initial data might lead to multiple EMV solutions. However, the scalar results also suggest some possible stability with respect to perturbations of atomic initial data. Based on these considerations, we propose the following (weaker) notion of stability.

Terminology 3.4. The MV Cauchy problem (2.3) is MV stable if the following property holds.

For every $u_0 \in L^\infty(\mathbb{R}^d, \mathbb{R}^N)$ and $\sigma \in \mathbf{Y}(\mathbb{R}^d, \mathbb{R}^N)$ such that

$$\mathcal{D}(\delta_{u_0}, \sigma) \ll 1,$$

there exists an EMV solution $\nu \in \mathcal{E}(\delta_{u_0})$ such that

$$\mathcal{D}(\nu, \nu^\sigma) \ll 1$$

for every EMV solution $\nu^\sigma \in \mathcal{E}(\sigma)$ (or a subset thereof).

(Recall that $\mathcal{E}(\sigma)$ denotes the set of all entropy MV solutions to the MV Cauchy problem (2.3).) We have intentionally left out several details in the above definition: the admissible set of initial data; the subset of $\mathcal{E}(\cdot)$ for which the MV Cauchy problem is stable; and the distance \mathcal{D} on the set of Young measures. Still, the concept of MV stability carries one of the main messages in this paper: despite the well-documented instability of entropic weak solutions, as shown for example in the introduction and in Section 6, one could still hope for a stable solution of systems of conservation laws, when it is interpreted as a measure-valued solution, subject to atomic initial data.

Carrying out the full scope of this paradigm for general systems of conservation laws is currently beyond reach. Instead, we examine the question of whether EMV solutions of selected systems of conservation laws are stable or not with the aid of numerical experiments reported in Section 6. As for the analytical aspects, we recall that in the scalar case, measure-valued perturbations of atomic initial data are stable (Theorem 3.3). In the following theorem we prove the MV stability in the case of systems, provided we further limit ourselves to MV perturbations of classical solutions of (2.3). The proof, similar to [20, Theorem 2.2], implies weak-strong uniqueness, as in [9]. In particular, the theorem provides consistency of EMV solutions with classical solutions of (1.1), as long as the latter exists.

Theorem 3.5. Assume that there exists a classical solution $u \in W^{1,\infty}(\mathbb{R}^d \times \mathbb{R}_+, \mathbb{R}^N)$ of (1.1) with initial data u_0 , both taking values in a compact set $K \subset \mathbb{R}^N$. Let ν be an EMV solution of (2.3) such that the support of both ν and its initial MV data σ are contained in K . Assume that η is uniformly convex on K . Then for all $t > 0$,

$$\int_{\mathbb{R}^d} \langle \nu_{(x,t)}, |u(x,t) - \xi|^2 \rangle dx \leq C(1 + te^{Ct}) \int_{\mathbb{R}^d} \langle \sigma_x, |u_0(x) - \xi|^2 \rangle dx,$$

or equivalently,

$$\left\| W_2(\nu_{(\cdot,t)}, \delta_{u(\cdot,t)}) \right\|_{L^2(\mathbb{R}^d)} \leq C(1 + te^{Ct}) \left\| W_2(\sigma, \delta_{u_0}) \right\|_{L^2(\mathbb{R}^d)}.$$

In particular, if $\sigma = \delta_{u_0}$ then $\nu = \delta_u$, and so any (classical, weak or measure-valued) solution must coincide with u .

Proof. Denote $\bar{u} := \langle \nu, \text{id} \rangle$ and $\bar{u}_0 := \langle \sigma, \text{id} \rangle$. Define the entropy variables $v = v(x,t) := \eta'(u(x,t))$ and denote $v_0 := v(x,0) = \eta'(u_0)$. It is readily verified that $v_t = -(f^i)'(u) \partial_i v$ (where $\partial_i = \frac{\partial}{\partial x_i}$). Here and in the remainder we use the Einstein summation convention.

Subtracting (2.4) from (1.2) and putting $\varphi(x,t) = v(x,t)\theta(t)$ for some $\theta \in C_c^1(\mathbb{R}_+)$ gives

$$\begin{aligned} 0 &= \int_{\mathbb{R}_+} \int_{\mathbb{R}^d} (\bar{u} - u) \cdot (v_t \theta + v \theta') + (\langle \nu, f^i \rangle - f^i(u)) \cdot \partial_i v \theta dx dt + \int_{\mathbb{R}^d} (\bar{u}_0 - u_0) \cdot v_0 \theta(0) dx \\ &= \int_{\mathbb{R}_+} \int_{\mathbb{R}^d} (\bar{u} - u) \cdot v \theta' + \underbrace{(\langle \nu, f^i \rangle - f^i(u) - (f^i)'(u)(\bar{u} - u))}_{=: Z^i} \cdot \partial_i v \theta dx dt + \int_{\mathbb{R}^d} (\bar{u}_0 - u_0) \cdot v_0 \theta(0) dx \end{aligned}$$

Next, note that since u is a classical solution, the entropy inequality (1.3) is in fact an equality. Hence, subtracting (2.6) from (1.3) and putting $\varphi(x,t) = \theta(t)$ gives

$$0 \leq \int_{\mathbb{R}_+} \int_{\mathbb{R}^d} (\langle \nu, \eta \rangle - \eta(u)) \theta' dx dt + \int_{\mathbb{R}^d} (\langle \sigma, \eta \rangle - \eta(u_0)) \theta(0) dx.$$

Subtracting these two expressions thus gives

$$0 \leq \int_{\mathbb{R}_+} \int_{\mathbb{R}^d} \hat{\eta} \theta' - Z^i \cdot \partial_i v \theta dx dt + \int_{\mathbb{R}^d} \hat{\eta}_0 \theta(0) dx. \quad (3.1)$$

where

$$\hat{\eta} := \langle \nu, \eta \rangle - \eta(u) - (\bar{u} - u) \cdot v, \quad \hat{\eta}_0 := \langle \sigma, \eta \rangle - \eta(u_0) - (\bar{u}_0 - u_0) \cdot v_0.$$

Let $\delta > 0$, and let $t > 0$ be a Lebesgue point for the function $s \mapsto \int_{\mathbb{R}} \hat{\eta}(x,s) dx$. We define

$$\theta(s) := \begin{cases} 1 & s < t \\ 1 - \frac{s-t}{\delta} & t \leq s < t + \delta \\ 0 & t + \delta \leq s. \end{cases}$$

Taking the limit $\delta \rightarrow 0$ in (3.1) then gives

$$\int_{\mathbb{R}^d} \hat{\eta}(t,x) dx \leq - \int_0^t \int_{\mathbb{R}^d} Z^i \cdot \partial_i v dx ds + \int_{\mathbb{R}^d} \hat{\eta}_0 dx.$$

Since $\nu_{(x,s)}$ is a probability distribution, it follows from the uniform convexity of η that

$$\hat{\eta} = \int_K \eta(\xi) - \eta(u) - \eta'(u) \cdot (\xi - u) \, d\nu \geq c \int_K |u - \xi|^2 \, d\nu = c \langle \nu, |u - \xi|^2 \rangle.$$

Similarly, by the L^∞ bound on both u and $\partial_i v$, we have

$$\hat{\eta}_0 \leq C \langle \sigma, |u_0 - \xi|^2 \rangle \quad \text{and} \quad |Z^i \cdot \partial_i v| \leq C \langle \nu, |u - \xi|^2 \rangle.$$

Hence,

$$\int_{\mathbb{R}^d} \langle \nu_{(x,t)}, |u - \xi|^2 \rangle \, dx \leq C \int_0^t \int_{\mathbb{R}} \langle \nu, |u - \xi|^2 \rangle \, dx ds + C \int_{\mathbb{R}^d} \langle \sigma, |u_0 - \xi|^2 \rangle \, dx.$$

By the integral form of Grönwall's lemma, we obtain the desired result. \square

Remark 3.6. In addition to proving consistency of entropy measure valued solutions with classical solutions (when they exist), the above theorem also provides local (in time) uniqueness of MV solutions in the following sense. Let $u_0 \in W^{1,\infty}(\mathbb{R}^d, \mathbb{R}^n)$ be the initial data in (1.1), then by standard results [17], we have local (in time) existence of a unique classical solution $u \in W^{1,\infty}(\mathbb{R}^d \times \mathbb{R}_+, \mathbb{R}^d)$. By the above theorem, δ_u is also the unique EMV solution of the MV Cauchy problem (2.3) with initial data δ_{u_0} . However, uniqueness can break down once this MV solution develops singularities.

4 Construction of approximate EMV solutions

Although existence results for specific systems of conservation laws such as polyconvex elastodynamics [20], two-phase flows [30, 31] and transport equations [12] are available, there exists no global existence result for a generic system of conservation laws. We pursue a different approach by constructing approximate EMV solutions and proving their convergence. A procedure for constructing approximate EMS is outlined in the present section. It provides a constructive proof of existence of EMV solutions for a generic system of conservation laws, and it is implemented in the numerical simulations reported in Section 6.

4.1 Numerical approximation of EMV solutions

The construction of approximate EMV solutions consists of several ingredients. It begins with a proper choice of a numerical scheme for approximating the system of conservation laws (1.1).

4.1.1 Numerical schemes for one- and multi-dimensional conservation laws

For simplicity, we begin with the description of a numerical scheme for a one-dimensional system of conservation laws, (1.1) with $d = 1$. We discretize our computational domain with into cells $\mathcal{C}_i := [x_{i-1/2}, x_{i+1/2})$ with mesh size $\Delta x = x_{i+1/2} - x_{i-1/2}$ with midpoints

$$x_i := \frac{x_{i-1/2} + x_{i+1/2}}{2}.$$

Note that we consider a uniform mesh size Δx only for the sake of simplicity of the exposition. Next, we discretize the one-dimensional system, $\partial_t u + \partial_x f(u) = 0$, with the following semi-discrete finite difference scheme for $u_i^{\Delta x}(t) \equiv u^{\Delta x}(x_i, t)$, [35, 48]:

$$\begin{aligned} \frac{d}{dt} u_i^{\Delta x}(t) + \frac{1}{\Delta x} \left(F_{i+1/2}^{\Delta x}(t) - F_{i-1/2}^{\Delta x}(t) \right) &= 0 \quad t > 0, \quad i \in \mathbb{Z} \\ u_i^{\Delta x}(0) &= u_0^{\Delta x}(x_i) \quad i \in \mathbb{Z}. \end{aligned} \quad (4.1a)$$

Here, $u_0^{\Delta x}$ is an approximation to the initial data u_0 . Henceforth, the dependence of u and F on Δx will be suppressed for notational convenience. The numerical flux function $F_{i+1/2}(t)$ is a function depending on $u(x_j, t)$ for $j = i - p + 1, \dots, i + p$ for some $p \in \mathbb{N}$. It is assumed to be consistent with f and locally Lipschitz continuous, i.e., for every compact $K \subset \mathbb{R}^N$ there is a $C > 0$ such that

$$|F_{i+1/2}(t) - f(u_i(t))| \leq C \sum_{j=i-p+1}^{i+p} |u_j - u_i|$$

whenever $u(x_j, t) \in K$ for $j = i - p + 1, \dots, i + p$.

The semi-discrete scheme (4.1a) needs to be integrated in time to define a fully discrete numerical approximation. Again for simplicity, we will use an exact time integration, resulting in

$$u_i^{\Delta x}(t + \Delta t) = u_i^{\Delta x}(t) - \frac{1}{\Delta x} \int_t^{t+\Delta t} (F_{i+1/2}(\tau) - F_{i-1/2}(\tau)) \, d\tau. \quad (4.1b)$$

The function $t \mapsto u(x_i, t)$ is then Lipschitz, that is,

$$|u^{\Delta x}(x_i, t) - u^{\Delta x}(x_i, s)| \leq \frac{C}{\Delta x} |t - s| \quad \forall i \in \mathbb{Z}, \quad t, s \in [0, T].$$

In particular, for all $\Delta x > 0$ and $i \in \mathbb{N}$, the function $t \mapsto u(x_i, t)$ is differentiable almost everywhere. We denote the evolution operator associated with the one-dimensional scheme (4.1) with mesh size Δx by $\mathcal{S}^{\Delta x}$, so that $u^{\Delta x} = \mathcal{S}^{\Delta x} u_0$.

A similar framework applies to systems of conservation laws in several space dimensions. To simplify the notation we restrict ourselves to the two-dimensional case (with the usual relabeling $(x_1, x_2) \mapsto (x, y)$), $\partial_t u + \partial_x f^x(u) + \partial_y f^y(u) = 0$.

We discretize our two-dimensional computational domain with into cells with mesh size $\Delta := (\Delta x_1, \Delta x_2)$: with the usual relabeling $(\Delta x_1, \Delta x_2) \mapsto (\Delta x, \Delta y)$, these two-dimensional cells, $\mathcal{C}_{i,j} := [x_{i-1/2}, x_{i+1/2}] \times [y_{j-1/2}, y_{j+1/2}]$ are assumed to have a fixed mesh ratio, $\Delta x = x_{i+1/2} - x_{i-1/2}$ and $\Delta y = y_{j+1/2} - y_{j-1/2}$ such that $\Delta y = c\Delta x$ for some constant c . Let

$$(x_i, y_j) = \left(\frac{x_{i-1/2} + x_{i+1/2}}{2}, \frac{y_{j-1/2} + y_{j+1/2}}{2} \right)$$

denote the mid-cells. We end up with the following semi-discrete finite difference scheme for $u_{ij}^{\Delta x, \Delta y} = u^{\Delta x, \Delta y}(x_i, y_j, t)$, [48, 35]:

$$\begin{aligned} \frac{d}{dt} u_{ij}^{\Delta x, \Delta y}(t) + \frac{1}{\Delta x} \left(F_{i+1/2, j}^{x, \Delta x}(t) - F_{i-1/2, j}^{x, \Delta x}(t) \right) + \frac{1}{\Delta y} \left(F_{i, j+1/2}^{y, \Delta y}(t) - F_{i, j-1/2}^{y, \Delta y}(t) \right) &= 0, \quad t > 0, \\ u_{ij}^{\Delta x, \Delta y}(0) &= u_0^{\Delta x, \Delta y}(x_i, y_j) \quad i \in \mathbb{Z}. \end{aligned} \quad (4.2a)$$

Here, $u_0^{\Delta x, \Delta y} \approx u_0$ is the approximate initial data and $F_{i+1/2, j}^{x, \Delta x}, F_{i, j+1/2}^{y, \Delta y}$ are the locally Lipschitz numerical flux functions which are assumed to be consistent with the flux function $f = (f^x, f^y)$. We integrate the semi-discrete scheme (4.2a) exactly in time to obtain,

$$\begin{aligned} u_{ij}^{\Delta x, \Delta y}(t + \Delta t) = & u_{ij}^{\Delta x, \Delta y}(t) - \frac{1}{\Delta x} \int_t^{t+\Delta t} \left(F_{i+1/2, j}^{x, \Delta x}(\tau) - F_{i-1/2, j}^{x, \Delta x}(\tau) \right) d\tau \\ & - \frac{1}{\Delta y} \int_t^{t+\Delta t} \left(F_{i, j+1/2}^{y, \Delta y}(\tau) - F_{i, j-1/2}^{y, \Delta y}(\tau) \right) d\tau. \end{aligned} \quad (4.2b)$$

We denote the evolution operator corresponding to (4.2) and associated with the two dimensional mesh $\Delta := (\Delta x_1, \Delta x_2)$ by \mathcal{S}^Δ .

4.1.2 Narrowly convergent schemes

The next ingredient in the construction of approximate EMV solutions for (2.3) is to employ the above numerical schemes in the following three step algorithm.

Algorithm 4.1.

Step 1: Let $u_0 : \Omega \mapsto L^\infty(\mathbb{R}^d)$ be a random field on a probability space (Ω, \mathcal{F}, P) such that the initial Young measure σ in (2.3) is the law of the random field u_0 (see Proposition A.3).

Step 2: We evolve the initial random field by applying the numerical scheme (4.1a) for every $\omega \in \Omega$ to obtain an approximation $u^{\Delta x}(\omega) := \mathcal{S}^{\Delta x} u_0(\omega)$ to the solution random field $u(\omega)$, corresponding to the initial random field $u_0(\omega)$.

Step 3: Define the approximate measure-valued solution $\nu^{\Delta x}$ as the law of $u^{\Delta x}$, see Appendix A.3.1.

By Proposition A.2 (Appendix A.3.1), $\nu^{\Delta x}$ is a Young measure. This sequence of Young measures $\nu^{\Delta x}$ serve as approximations to the EMV solutions of (2.3).

Next, we show that if the numerical scheme (4.1a) satisfies a set of criteria, then the approximate Young measures $\nu^{\Delta x}$ generated by Algorithm 4.1 will converge narrowly to an EMV solution of (2.3). Specific examples for such narrowly convergent schemes is provided in Section 5. To simplify the presentation, we restrict attention to the one-dimensional case; the argument in the general multi-dimensional case can be found in [26].

Theorem 4.2. Assume that the approximate solutions $u^{\Delta x}$ generated by the one-dimensional numerical scheme (4.1) satisfy the following:

- Uniform boundedness:

$$\|u^{\Delta x}(\omega)\|_{L^\infty(\mathbb{R} \times \mathbb{R}_+)} \leq C, \quad \forall \omega \in \Omega, \Delta x > 0. \quad (4.3a)$$

- Weak BV: There exists $1 \leq r < \infty$ such that

$$\lim_{\Delta x \rightarrow 0} \int_0^T \sum_i |u_{i+1}^{\Delta x}(\omega, t) - u_i^{\Delta x}(\omega, t)|^r \Delta x dt = 0 \quad \forall \omega \in \Omega \quad (4.3b)$$

- Entropy consistency: The numerical scheme (4.1a) is entropy stable with respect to an entropy pair (η, q) i.e, there exists a numerical entropy flux $Q = Q_{i+1/2}(t)$, consistent with the entropy flux q and locally Lipschitz, such that computed solutions satisfy the discrete entropy inequality

$$\frac{d}{dt}\eta(u^{\Delta x}) + \frac{1}{\Delta x} \left(Q_{i+1/2}^{\Delta x} - Q_{i-1/2}^{\Delta x} \right) \leq 0 \quad \forall t > 0, i \in \mathbb{Z}, \omega \in \Omega. \quad (4.3c)$$

- Consistency with initial data: If $\sigma^{\Delta x}$ is the law of $u_0^{\Delta x}$, then

$$\lim_{\Delta x \rightarrow 0} \int_{\mathbb{R}} \psi(x) \langle \sigma_x^{\Delta x}, \text{id} \rangle dx = \int_{\mathbb{R}} \psi(x) \langle \sigma_x, \text{id} \rangle dx \quad \forall \psi \in C_c^1(\mathbb{R}). \quad (4.3d)$$

and

$$\limsup_{\Delta x \rightarrow 0} \int_{\mathbb{R}} \psi(x) \langle \sigma_x^{\Delta x}, \eta \rangle dx \leq \int_{\mathbb{R}} \psi(x) \langle \sigma_x, \eta \rangle dx \quad \forall 0 \leq \psi \in C_c^1(\mathbb{R}) \quad (4.3e)$$

Then the approximate Young measures $\nu^{\Delta x}$ converge narrowly (up to a subsequence) as $\Delta x \rightarrow 0$, to an EMV solution $\nu \in \mathbf{Y}(\mathbb{R} \times \mathbb{R}_+, \mathbb{R}^N)$ of (2.3).

Proof. From the assumption (4.3a) that $u^{\Delta x}$ is L^∞ -bounded, it follows that $\nu^{\Delta x}$ is compactly supported, in the sense that its support $\text{supp } \nu_{(x,t)}^{\Delta x}$ lies in a fixed compact subset of \mathbb{R}^N for every (x, t) ; see Appendix A.2.2. The fundamental theorem of Young measures (see Appendix A.2.6) gives the existence of a $\nu \in \mathbf{Y}(\mathbb{R}^d \times \mathbb{R}_+, \mathbb{R}^N)$ and a subsequence of $\nu^{\Delta x}$ such that $\nu^{\Delta x} \rightharpoonup \nu$ narrowly

First, we show that the limit Young measure ν satisfies the entropy inequality (2.6). To this end, let $\varphi \in C_c^1(\mathbb{R} \times [0, T])$. Then

$$\begin{aligned} & \int_0^T \int_{\mathbb{R}^d} \langle \nu_{(x,t)}, \eta \rangle \partial_t \varphi(x, t) + \langle \nu_{(x,t)}, q \rangle \partial_x \varphi(x, t) dx dt \\ &= \lim_{\Delta x \rightarrow 0} \int_0^T \int_{\mathbb{R}^d} \langle \nu_{(x,t)}^{\Delta x}, \eta \rangle \partial_t \varphi(x, t) + \langle \nu_{(x,t)}^{\Delta x}, q \rangle \partial_x \varphi(x, t) dx dt \end{aligned}$$

by the narrow convergence $\nu^{\Delta x} \rightharpoonup \nu$. Denote $\eta^{\Delta x}(\omega, x, t) := \eta(u^{\Delta x}(\omega, x, t))$. Then for every

$\Delta x > 0$ we have

$$\begin{aligned}
& \int_0^T \int_{\mathbb{R}^d} \langle \nu_{(x,t)}^{\Delta x}, \eta \rangle \partial_t \varphi(x,t) \, dx dt + \int_{\mathbb{R}^d} \varphi(x,0) \langle \sigma_x^{\Delta x}, \eta \rangle \, dx = \int_{\mathbb{R}} \int_0^T -\partial_t \langle \nu_{(x,t)}^{\Delta x}, \eta \rangle \varphi(x,t) \, dt dx \\
&= \int_{\Omega} \int_{\mathbb{R}} \int_0^T -\partial_t \eta^{\Delta x}(\omega, x, t) \varphi(x,t) \, dt dx dP(\omega) \\
&\geq \int_{\Omega} \int_{\mathbb{R}} \int_0^T \sum_i \mathbb{1}_{\mathcal{C}_i}(x) \frac{Q_{i+1/2}(\omega, t) - Q_{i-1/2}(\omega, t)}{\Delta x} \varphi(x,t) dt dx dP(\omega) \\
&= \int_{\Omega} \int_0^T \sum_i \frac{Q_{i+1/2}(\omega, t) - Q_{i-1/2}(\omega, t)}{\Delta x} \int_{\mathcal{C}_i} \varphi(x,t) \, dx dt dP(\omega) \\
&= \int_{\Omega} \int_0^T \sum_i (Q_{i+1/2}(\omega, t) - Q_{i-1/2}(\omega, t)) \bar{\varphi}_i^{\Delta x}(t) \, dt dP(\omega) \\
&= - \int_{\Omega} \int_0^T \sum_i Q_{i+1/2}(\omega, t) \frac{\bar{\varphi}_{i+1}^{\Delta x}(t) - \bar{\varphi}_i^{\Delta x}(t)}{\Delta x} \, \Delta x dt dP(\omega) \\
&= - \int_{\Omega} \int_0^T \sum_i q(u_i^{\Delta x}(\omega, t)) \frac{\bar{\varphi}_{i+1}^{\Delta x}(t) - \bar{\varphi}_i^{\Delta x}(t)}{\Delta x} \, \Delta x dt dP(\omega) \\
&\quad - \int_{\Omega} \int_0^T \sum_i (Q_{i+1/2}(\omega, t) - q(u_i^{\Delta x}(\omega, t))) \frac{\bar{\varphi}_{i+1}^{\Delta x}(t) - \bar{\varphi}_i^{\Delta x}(t)}{\Delta x} \, \Delta x dt dP(\omega).
\end{aligned}$$

(We have written $\bar{\varphi}_i^{\Delta x}(t) := \frac{1}{\Delta x} \int_{\mathcal{C}_i} \varphi(x,t) \, dx$.) The first term can be written as

$$\begin{aligned}
& - \int_{\Omega} \int_0^T \sum_i q(u_i^{\Delta x}(\omega, t)) \frac{\bar{\varphi}_{i+1}^{\Delta x}(t) - \bar{\varphi}_i^{\Delta x}(t)}{\Delta x} \, \Delta x dt = - \int_0^T \sum_i \langle \nu_{(x,t)}^{\Delta x}, q \rangle \frac{\bar{\varphi}_{i+1}^{\Delta x}(t) - \bar{\varphi}_i^{\Delta x}(t)}{\Delta x} \, \Delta x dt dP(\omega) \\
&\quad \rightarrow - \int_0^T \int_{\mathbb{R}} \langle \nu_{(x,t)}, q \rangle \partial_x \varphi(x,t) \, dx dt.
\end{aligned}$$

The second term goes to zero:

$$\begin{aligned}
& \left| \int_{\Omega} \int_0^T \sum_i (Q_{i+1/2}(\omega, t) - q(u_i^{\Delta x}(\omega, t))) \frac{\bar{\varphi}_{i+1}^{\Delta x}(t) - \bar{\varphi}_i^{\Delta x}(t)}{\Delta x} \, \Delta x dt dP(\omega) \right| \\
&\leq C \int_{\Omega} \int_0^T \sum_i |u_{i+1}^{\Delta x}(\omega, t) - u_i^{\Delta x}(\omega, t)| \left| \frac{\bar{\varphi}_{i+1}^{\Delta x}(t) - \bar{\varphi}_i^{\Delta x}(t)}{\Delta x} \right| \, \Delta x dt dP(\omega) \\
&\leq C \sup_{\omega} \left(\int_0^T \sum_i |u_{i+1}^{\Delta x}(\omega, t) - u_i^{\Delta x}(\omega, t)|^r \, \Delta x dt \right)^{1/r} \|\partial_x \varphi\|_{L^{r'}(\mathbb{R} \times (0,T))} \\
&\rightarrow 0
\end{aligned}$$

by (4.3b), where r' is the conjugate exponent of r . In conclusion, the limit ν satisfies (2.6).

The proof that the limit measure ν satisfies (2.4) follows from the above by setting $\eta = \pm \text{id}$ and $q = \pm f$. \square

A similar construction can be readily performed in several space dimensions. To this end, we replace $S^{\Delta x}$ in Step 2 of Algorithm 4.1 with the two-dimensional solution operator S^Δ , and the corresponding approximate solution $u^{\Delta x}$ with u^Δ . The narrow convergence of the resulting approximate young measure ν^Δ is described below.

Theorem 4.3. Assume that the approximate solutions $u^{\Delta x}$ generated by scheme (4.2a) satisfy the following:

- Uniform boundedness:

$$\|u^{\Delta x}(\omega)\|_{L^\infty(\mathbb{R}^2 \times \mathbb{R}_+)} \leq C, \quad \forall \omega \in \Omega, \Delta x, \Delta y > 0. \quad (4.4)$$

- Weak BV: There exist $1 \leq r < \infty$ such that

$$\lim_{\Delta x, \Delta y \rightarrow 0} \int_0^T \sum_{i,j} \left(|u_{i+1,j}^{\Delta x}(\omega, t) - u_{i,j}^{\Delta x}(\omega, t)|^r + |u_{i,j+1}^{\Delta x}(\omega, t) - u_{i,j}^{\Delta x}(\omega, t)|^r \right) \Delta x \Delta y dt = 0 \quad \forall \omega \in \Omega \quad (4.5)$$

- Entropy consistency: The numerical scheme (4.2a) is entropy stable with respect to an entropy pair (η, q) i.e, there exists locally Lipschitz numerical entropy fluxes $(Q^x, Q^y) = (Q_{i+1/2,j}^x(t), Q_{i,j+1/2}^y(t))$, consistent with the entropy flux $q = (q^x, q^y)$, such that computed solutions satisfy the discrete entropy inequality

$$\frac{d}{dt} \eta(u^{\Delta x}) + \frac{1}{\Delta x} \left(Q_{i+1/2,j}^{x,\Delta x} - Q_{i-1/2,j}^{x,\Delta x} \right) + \frac{1}{\Delta y} \left(Q_{i,j+1/2}^{y,\Delta x} - Q_{i,j-1/2}^{y,\Delta x} \right) \leq 0 \quad \forall t > 0, i, j \in \mathbb{Z}, \omega \in \Omega. \quad (4.6)$$

- Consistency with initial data: Let $\sigma^{\Delta x}$ be the law of the random field $u_0^{\Delta x}$ that approximates the initial random field u_0 . Then, the consistency conditions (4.3d) and (4.3e) hold.

Then, the approximate Young measures ν^Δ converge narrowly (up to a subsequence) to a Young measure $\nu \in \mathbf{Y}(\mathbb{R}^2 \times \mathbb{R}_+, \mathbb{R}^N)$ as $\Delta x, \Delta y \rightarrow 0$ and ν is an EMV solution of (2.3) i.e,

The proof of the above theorem is a simple generalization of the proof of convergence theorem 4.2. The above construction can also be readily extended to three spatial dimensions.

Remark 4.4. The uniform L^∞ bound (4.3a),(4.4) is a technical assumption that we require in this article. This assumption can be relaxed to only an L^p bound. This extension is described in a forthcoming paper [27].

Remark 4.5. The conditions (4.3d) and (4.3e), which say that $\sigma^{\Delta x} \rightarrow \sigma$ in a certain sense, are weaker than narrow convergence. It is readily checked that a sufficient condition for this is that $u_0 \in L^1(\mathbb{R}; \mathbb{R}^N) \cap L^\infty(\mathbb{R}; \mathbb{R}^N)$ and $u_0^{\Delta x}(\omega, \cdot) \rightarrow u_0(\omega, \cdot)$ in $L^1(\mathbb{R}^d; \mathbb{R}^N)$ for all $\omega \in \Omega$ (which in fact implies that $\sigma^{\Delta x} \rightarrow \sigma$ strongly).

4.1.3 Narrow convergence with atomic initial data

In view of the nonuniqueness example 3.2, one can not expect an unique construction of EMV solutions for general MV initial data. Instead, as argued before, we focus attention on perturbation of atomic initial data $\sigma = \delta_{u_0}$ for some $u_0 \in L^1(\mathbb{R}^d, \mathbb{R}^N) \cap L^\infty(\mathbb{R}^d, \mathbb{R}^N)$. We construct approximate EMV solutions of (2.3) in this case using the following specialization of Algorithm 4.1.

Algorithm 4.6. Let (Ω, \mathcal{F}, P) be a probability space and let $X : \Omega \rightarrow L^1(\mathbb{R}^d) \cap L^\infty(\mathbb{R}^d)$ be a random variable satisfying $\|X\|_{L^1(\mathbb{R}^d)} \leq 1$ P -almost surely.

Step 1: Fix a small number $\varepsilon > 0$. Perturb u_0 by defining $u_0^\varepsilon(\omega, x) := u_0(x) + \varepsilon X(\omega, x)$. Let σ^ε be the law of u_0^ε .

Step 2: For each $\omega \in \Omega$ and $\varepsilon > 0$, let $u^{\Delta x, \varepsilon}(\omega) := \mathcal{S}^{\Delta x} u_0^\varepsilon(\omega)$, with $\mathcal{S}^{\Delta x}$ being the solution operator corresponding to the numerical scheme (4.1).

Step 3: Let $\nu^{\Delta x, \varepsilon}$ be the law of $u^{\Delta x, \varepsilon}$. □

Theorem 4.7. Let $\{\nu^{\Delta x, \varepsilon}\}$ be the family approximate EMV solutions constructed by Algorithm 4.6. Then there exists a subsequence $(\Delta x_n, \varepsilon_n) \rightarrow 0$ such that

$$\nu^{\Delta x_n, \varepsilon_n} \rightharpoonup \nu \in \mathcal{E}(\delta_{u_0}),$$

that is, $\nu^{\Delta x_n, \varepsilon_n}$ converges narrowly to an EMV solution ν with atomic initial data u_0 .

Proof. By Theorem 4.2 we know that for every $\varepsilon > 0$ there exists a subsequence $\nu^{\Delta x_n, \varepsilon}$ which converges narrowly to an EMV solution ν^ε of (2.3) with initial data σ^ε . Thus, (2.6) holds with (ν, σ) replaced by $(\nu^\varepsilon, \sigma^\varepsilon)$; we abbreviate the corresponding entropy statement as $(2.6)_\varepsilon$. The convergence of the sequence ν^{ε_n} as $\varepsilon_n \rightarrow 0$ is a consequence of the fundamental theorem of Young measures: by Theorem A.1, there exists a narrowly convergent subsequence $\nu^{\varepsilon_n} \rightharpoonup \nu$. The fact that ν is an EMV solution follows at once by taking the limit $\varepsilon_n \rightarrow 0$ in $(2.6)_{\varepsilon_n}$. □

4.2 What are we computing – narrow convergence of space-time averages

We begin by quoting [46, p. 143]: “Just because we cannot prove that compressible flows with prescribed initial values exist doesn’t mean that we cannot compute them”. The question is what are the computed quantities encoded in the EMV solutions.

According to Theorems 4.2, 4.7, the approximations generated by Algorithm 4.1 and 4.5 converge to an EMV solution in the following sense: for all $g \in C_0(\mathbb{R}^N)$ and $\psi \in L^1(\mathbb{R}^d \times \mathbb{R}_+)$,

$$\lim_{\Delta x \rightarrow 0} \int_{\mathbb{R}_+} \int_{\mathbb{R}^d} \psi(x, t) \langle \nu_{(x,t)}^{\Delta x}, g \rangle dx dt = \int_{\mathbb{R}_+} \int_{\mathbb{R}^d} \psi(x, t) \langle \nu_{(x,t)}, g \rangle dx dt. \quad (4.7)$$

As we assume that the approximate solutions are L^∞ -bounded (property (4.3a)), any $g \in C(\mathbb{R}^N)$ can serve as a test function in (4.7); see Appendix A.2.6. In particular, we can choose $g(\xi) = \xi$ to obtain the mean of the measure valued solution. Similarly, the variance can be computed by choosing the test function $g(\xi) = \xi \otimes \xi$. Higher statistical moments can

be computed analogously.

In practice, the goal of any numerical simulation is to accurately compute statistics of space-time averages or statistics of functionals of interest of solution variables and to compare them to experimental or observational data. Thus, the narrow convergence of approximate Young measures, computed by Algorithms 4.1 and 4.5 provides an approximation of exactly these observable quantities of interest.

4.2.1 Monte Carlo approximation

In order to compute statistics of space-time averages in (4.7), we need to compute phase space integrals with respect to the measure $\nu^{\Delta x}$:

$$\langle \nu_{(x,t)}^{\Delta x}, g \rangle := \int_{\mathbb{R}^N} g(\xi) d\nu_{(x,t)}^{\Delta x}(\xi).$$

The last ingredient in our construction of EMV solutions, therefore, is numerical approximation which is necessary to compute these phase space integrals. To this end, we utilize the equivalent representation of the measure $\nu^{\Delta x}$ as the law of the random field $u^{\Delta x}$:

$$\langle \nu_{(x,t)}^{\Delta x}, g \rangle := \int_{\mathbb{R}^N} g(\xi) d\nu_{(x,t)}^{\Delta x}(\xi) = \int_{\Omega} g(u^{\Delta x}(\omega; x, t)) dP(\omega). \quad (4.8)$$

We will approximate this integral by a Monte Carlo sampling procedure:

Algorithm 4.8. Let $\Delta x > 0$ and let M be a positive integer. Let $\sigma^{\Delta x}$ be the initial Young measure in (2.3) and let $u_0^{\Delta x}$ be a random field $u_0^{\Delta x} : \Omega \times \mathbb{R}^d \rightarrow \mathbb{R}^N$ such that $\sigma^{\Delta x}$ is the law of $u_0^{\Delta x}$.

Step 1: Draw M independent and identically distributed random fields $u_0^{\Delta x, k}$ for $k = 1, \dots, M$.

Step 2: For each k and for a fixed $\omega \in \Omega$, use the finite difference scheme (4.1a) to numerically approximate the conservation law (1.1) with initial data $u_0^{\Delta x, k}(\omega)$. Denote $u^{\Delta x, k}(\omega) = \mathcal{S}^{\Delta x} u_0^{\Delta x, k}(\omega)$.

Step 3: Define the approximate measure-valued solution

$$\nu^{\Delta x, M} := \frac{1}{M} \sum_{k=1}^M \delta_{u^{\Delta x, k}(\omega)}.$$

□

For every $g \in C(\mathbb{R}^N)$ we have

$$\langle \nu^{\Delta x, M}, g \rangle = \frac{1}{M} \sum_{k=1}^M g(u^{\Delta x, k}(\omega)).$$

Thus, the space-time average (4.7) is approximated by

$$\int_{\mathbb{R}_+} \int_{\mathbb{R}^d} \psi(x, t) \langle \nu_{(x,t)}^{\Delta x}, g \rangle dx dt \approx \frac{1}{M} \sum_{k=1}^M \int_{\mathbb{R}_+} \int_{\mathbb{R}^d} \psi(x, t) g(u^{\Delta x, k}(\omega; x, t)) dx dt. \quad (4.9)$$

Note that, as in any Monte Carlo method, the approximation $\nu^{\Delta x, M}$ depends on the choice of $\omega \in \Omega$, i.e., the choice of seed in the random number generator. However, we can prove that the quality of approximation is independent of this choice, P -almost surely:

Theorem 4.9 (Convergence for large samples). Algorithm 4.8 converges, that is,

$$\nu^{\Delta x, M} \rightharpoonup \nu^{\Delta x} \quad \text{narrowly,}$$

and, for a subsequence $M \rightarrow \infty$, P -almost surely. Equivalently, for every $\psi \in L^1(\mathbb{R}^d \times \mathbb{R}_+)$ and $g \in C(\mathbb{R}^N)$,

$$\lim_{M \rightarrow \infty} \frac{1}{M} \sum_{k=1}^M \int_{\mathbb{R}_+} \int_{\mathbb{R}^d} \psi(x, t) g(u^{\Delta x, k}(x, t)) dx dt = \int_{\mathbb{R}_+} \int_{\mathbb{R}^d} \psi(x, t) \langle \nu_{(x,t)}^{\Delta x}, g \rangle dx dt. \quad (4.10)$$

The limits are uniform in Δx .

The proof involves an adaptation of the law of large numbers for the present setup and is provided in Appendix B. Combining (4.10) with the convergence established in Theorem 4.2, we conclude with the following.

Corollary 4.10 (Convergence with mesh refinement). There are subsequences $\Delta x \rightarrow 0$ and $M \rightarrow \infty$ such that

$$\nu^{\Delta x, M} \rightharpoonup \nu \quad \text{narrowly,}$$

or equivalently, for every $\psi \in L^1(\mathbb{R}^d \times \mathbb{R}_+)$ and $g \in C(\mathbb{R}^N)$,

$$\lim_{\Delta x \rightarrow 0} \lim_{M \rightarrow \infty} \frac{1}{M} \sum_{k=1}^M \int_{\mathbb{R}_+} \int_{\mathbb{R}^d} \psi(x, t) g(u^{\Delta x, k}(x, t)) dx dt = \int_{\mathbb{R}_+} \int_{\mathbb{R}^d} \psi(x, t) \langle \nu_{(x,t)}, g \rangle dx dt \quad (4.11)$$

The limits in Δx and M are interchangeable.

5 Examples of narrowly convergent numerical schemes

In this section, we provide concrete examples of numerical schemes that satisfy the criteria (4.3) of Theorem 4.2, for narrow convergence to EMV solutions of (2.3).

5.1 Scalar conservation laws

We begin by considering scalar conservation laws. Monotone finite difference (volume) schemes (see [16, 35] for a precise definition) for scalar equations are uniformly bounded in L^∞ (as they satisfy a discrete maximum principle), satisfy a discrete entropy inequality (using the Crandall-Majda numerical entropy fluxes [16]) and are TVD – the total variation

of the approximate solutions is non-increasing over time. Consequently, the approximate solutions satisfy the weak BV estimate (4.3b) with $r = 1$. Thus, monotone schemes, approximating scalar conservation laws, satisfy all the abstract criteria of Theorem 4.2.

In fact, one can obtain a precise convergence rate for monotone schemes [44]:

$$\|u^{\Delta x}(\omega, \cdot, t) - u(\omega, \cdot, t)\|_{L^1(\mathbb{R}^d)} \leq Ct \text{TV}(u_0(\omega)) \sqrt{|\Delta x|} \quad \forall \omega, \quad (5.1)$$

where $u(\omega) = \lim_{\Delta x \rightarrow 0} u^{\Delta x}(\omega)$ denotes the entropy solution of the Cauchy problem for a scalar conservation law with initial data $u_0(\omega)$. Using this error estimate, we obtain the following strong convergence results for monotone schemes.

Theorem 5.1. Let $\nu^{\Delta x}$ be generated by Algorithm 4.1, and let ν be the law of the entropy solution $u(\omega)$. If $\text{TV}(u_0(\omega)) \leq C$ for all $\omega \in \Omega$, then $\nu^{\Delta x} \rightarrow \nu$ strongly as $\Delta x \rightarrow 0$.

Proof. Define $\pi_z^{\Delta x} \in \mathcal{P}(\mathbb{R}^N \times \mathbb{R}^N)$ as the law of the random variable $(u^{\Delta x}(z), u(z))$,

$$\pi_z^{\Delta x}(A) := P((u^{\Delta x}(z), u(z)) \in A), \quad A \subset \mathbb{R} \times \mathbb{R} \text{ Borel measurable.}$$

Then $\pi_z^{\Delta x}$ is a Young measure for all z and $\Delta x > 0$. Clearly, $\pi_z^{\Delta x} \in \Pi(\nu_z^{\Delta x}, \nu_z)$, and hence

$$W_1(\nu_z^{\Delta x}, \nu_z) \leq \int_{\mathbb{R}^N \times \mathbb{R}^N} |\xi - \zeta| d\pi(\xi, \zeta) = \int_{\Omega} |u^{\Delta x}(\omega, x, t) - u(\omega, x, t)| dP(\omega).$$

Hence, by Kutznetsov's error estimate (5.1),

$$\int_0^T \int_{\mathbb{R}} W_1(\nu_z^{\Delta x}, \nu_z) dx dt \leq C \sqrt{|\Delta x|} \rightarrow 0 \quad \text{as } \Delta x \rightarrow 0.$$

□

Remark 5.2. We can relax the uniform boundedness of $\text{TV}(u_0(\omega))$ to just integrability of the function $\omega \mapsto \text{TV}(u_0(\omega))$.

Remark 5.3. Note that, in light of Theorem 3.1 and Example 3.2, the limit entropy measure-valued solution ν is unique only if the initial measure-valued data σ is atomic.

5.2 Systems of conservation laws

We present two classes of schemes, approximating systems of conservation laws, that satisfy the convergence criteria (4.3) of Theorem 4.2. Again, although we discuss the one-dimensional setup, the arguments go through the multi-dimensional case.

5.2.1 TeCNO finite difference schemes

The TeCNO schemes, introduced in [25, 26], are finite difference schemes of the form (4.1a) with flux function

$$F_{i+1/2} := \tilde{F}_{i+1/2}^p - \frac{1}{2} D_{i+1/2} (v_{i+1}^- - v_i^+). \quad (5.2)$$

Here, $\tilde{F}_{i+1/2}^p$ is a p -th order accurate ($p \in \mathbb{N}$) entropy conservative numerical flux (see [60, 47]), $D_{i+1/2}$ is a positive definite matrix, and v_j^\pm are the cell interface values of a p -th order accurate ENO reconstruction of the entropy variable $v := \eta'(u)$ (see [37, 24]). It was shown in [25, 26] that the TeCNO schemes

- are (formally) p -th order accurate
- are entropy stable – they satisfy a discrete entropy inequality of the form (4.3c)
- have weakly bounded variation, i.e., they satisfy a bound of the form (4.3b).

Hence, under the assumption (4.3a) that the scheme is bounded in L^∞ , the approximate Young measures, generated by the TeCNO scheme, converge to an EMV solution of (2.3).

5.2.2 Shock capturing space time Discontinuous Galerkin (DG) schemes

Although suited for Cartesian grids, finite difference schemes of the type (4.1a) are difficult to extend to unstructured grids in several space dimensions. For problems with complex domain geometry that necessitates the use of unstructured grids (triangles, tetrahedra), an alternative discretization procedure is the space-time discontinuous finite element procedure of [41, 39, 5, 38]. In this procedure, the entropy variables serve as degrees of freedom and entropy stable numerical fluxes like (5.2) need to be used at cell interfaces. Further stabilization terms like streamline diffusion and shock capturing terms are also necessary. In a recent paper [38], it was shown that a shock capturing streamline diffusion space-time DG method satisfied a discrete entropy inequality and a suitable version of the weak BV bound (4.3b). Hence, this method was also shown to converge to an EMV solution in [38]. We remark that the space-time DG methods are fully discrete in contrast to semi-discrete finite difference schemes such as (4.1a).

6 Numerical Results

Our overall goal will be to compute approximate EMV solutions of (2.3) with atomic initial data, as well as investigating the stability of these solutions with respect to initial data. In Sections 6.1 and 6.2 we consider the Kelvin-Helmholtz instability problem (1.8). In Section 6.3 we consider the Richtmeyer-Meshkov instability problem, e.g., [34] and the references therein.

For the rest of the section, we will present numerical experiments for the two-dimensional compressible Euler equations

$$\frac{\partial}{\partial t} \begin{pmatrix} \rho \\ \rho w^x \\ \rho w^y \\ E \end{pmatrix} + \frac{\partial}{\partial x_1} \begin{pmatrix} \rho w^x \\ \rho(w^x)^2 + p \\ \rho w^x w^y \\ (E + p)w^x \end{pmatrix} + \frac{\partial}{\partial x_2} \begin{pmatrix} \rho w^y \\ \rho w^x w^y \\ \rho(w^y)^2 + p \\ (E + p)w^y \end{pmatrix} = 0. \quad (6.1)$$

Here, the density ρ , velocity field (w^x, w^y) , pressure p and total energy E are related by the equation of state

$$E = \frac{p}{\gamma - 1} + \frac{\rho((w^x)^2 + (w^y)^2)}{2}.$$

The relevant entropy pair is given by

$$\eta(u) = \frac{-\rho s}{\gamma - 1}, \quad q^1(u) = w^x \eta(u), \quad q^2(u) = w^y \eta(u).$$

with $s = \log(p) - \gamma \log(\rho)$ being the thermodynamic entropy. The adiabatic constant γ is set to 1.4.

6.1 Kelvin-Helmholtz problem: mesh refinement ($\Delta x \downarrow 0$)

As our first numerical experiment, we consider the two-dimensional compressible Euler equations of gas dynamics (6.1) with the initial data,

$$u_0(x, \omega) = \begin{cases} u_L & \text{if } I_1 < x_2 < I_2 \\ u_R & \text{if } x_2 \leq I_1 \text{ or } x_2 \geq I_2, \end{cases} \quad x \in [0, 1]^2 \quad (6.2)$$

with $\rho_L = 2$, $\rho_R = 1$, $w_L^x = -0.5$, $w_R^x = 0.5$, $w_L^y = w_R^y = 0$ and $p_L = p_R = 2.5$. The interface profiles

$$I_j = I_j(x, \omega) := J_j + \varepsilon Y_j(x, \omega), \quad j = 1, 2$$

are chosen to be small perturbations around $J_1 := 0.25$ and $J_2 := 0.75$, respectively, with

$$Y_j(x, \omega) = \sum_{n=1}^m a_j^n(\omega) \cos(b_j^n(\omega) + 2n\pi x_1), \quad j = 1, 2.$$

Here, $a_j^n = a_j^n(\omega) \in [0, 1]$ and $b_j^n = b_j^n(\omega) \in [0, 1]$, $i = 1, 2$, $n = 1, \dots, m$ are randomly chosen numbers. The coefficients a_j^n have been normalized such that $\sum_{n=1}^m a_j^n = 1$ to guarantee that $|I_j(x, \omega) - J_j| \leq \varepsilon$ for $j = 1, 2$. We set $m = 10$.

We observe that the resulting measure valued Cauchy problem involves a random perturbation of the interfaces between the two streams (jets). This should be contrasted with initial value problem (1.8), where the amplitude was randomly perturbed (1.5). We note that the law of the above initial datum can readily be written down and serves as the initial Young measure in the measure valued Cauchy problem (2.3). Observe that this Young measure is not atomic in the whole domain.

6.1.1 Lack of sample convergence

We approximate the above MV Cauchy problem with the second-order entropy stable TeCNO2 scheme of [25]. In Figure 6.1 we show the density at time $t = 2$ for a single sample, i.e, for a fixed $\omega \in \Omega$, at different grid resolutions, ranging from 128^2 points to 1024^2 points. The figure suggests that the approximate solutions do not seem to converge as the mesh is refined. In particular, finer and finer scale structures are formed as the mesh is refined, as already seen in Figure 1.3. To further verify this lack of convergence, we compute the L^1 difference of the approximate solutions at successive mesh levels (1.7) and present the results in Figure 6.2. We observe that this difference does not go to zero, suggesting that the approximate solutions do not converge as the mesh is refined.

6.1.2 Convergence of the mean and variance

The lack of convergence of the numerical schemes for single samples is not unexpected, given the results already mentioned in the introduction. Next, we will compute statistical quantities of the interest for this problem. First, we compute the Monte-Carlo approximation of the mean (4.9), denoted by $\bar{u}^{\Delta x}(x, t)$, at every point (x, t) in the computational domain. This sample mean of the density, computed with $M = 400$ samples and the second-order TeCNO2 scheme is presented in Figure 6.3 for different grid resolutions. The figure clearly

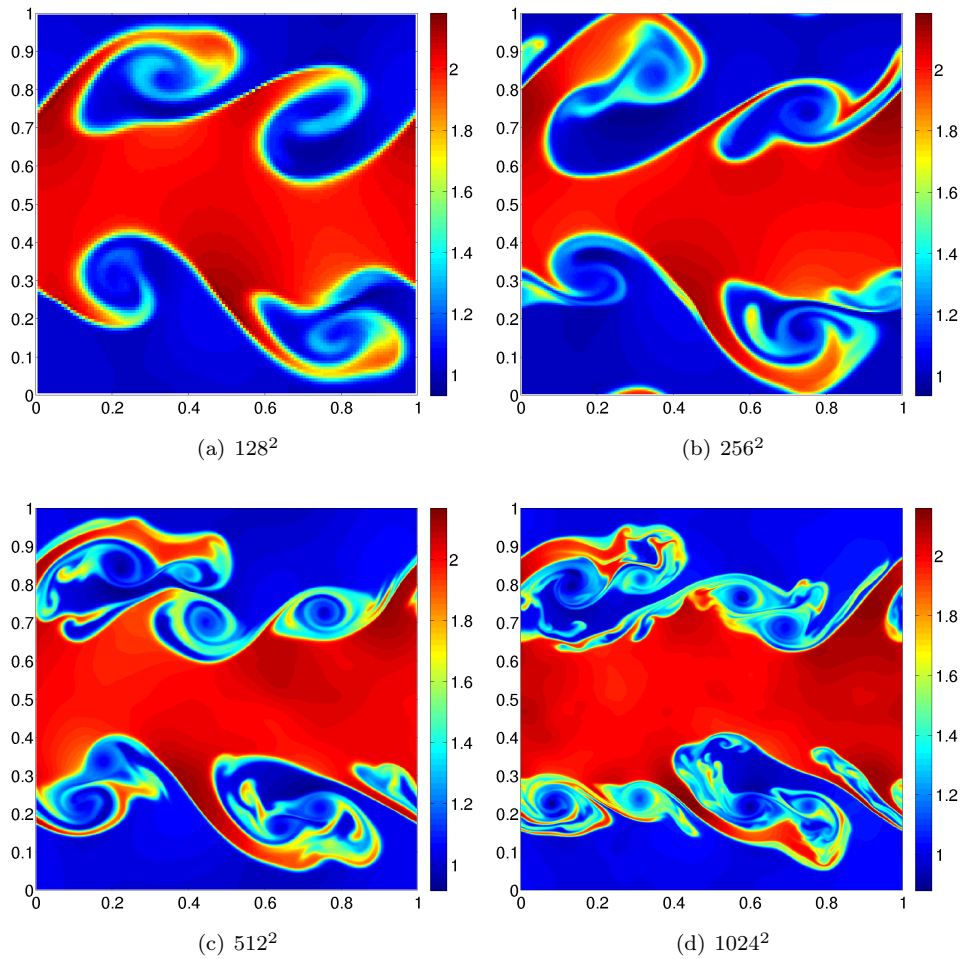


Figure 6.1: Approximate density for the Euler equations (6.1) with initial data (6.2), $\varepsilon = 0.01$ and for a fixed ω (single sample), computed with the second-order TeCNO2 scheme of [25], at time $t = 2$ at different mesh resolutions.

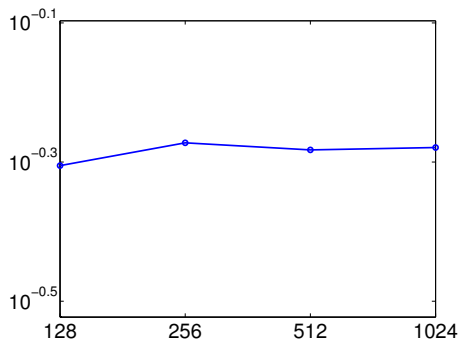


Figure 6.2: The Cauchy rates (1.7) at $t = 2$ for the density (y-axis) for a single sample of the Kelvin-Helmholtz problem, vs. different mesh resolutions (x-axis)

shows that the sample mean converges as the mesh is refined. This stands in stark contrast with the lack of convergence, at the level of single samples, as shown in Figure 1.3 and Figure 6.1. Furthermore, Figure 6.3 also reveals that small scale structures, present in single sample computations, are indeed smeared or averaged out in the mean. This convergence of the mean is further quantified by computing the L^1 difference of the mean,

$$\|\bar{u}^{\Delta x} - \bar{u}^{\Delta x/2}\|_{L^1([0,1]^2)}. \quad (6.3)$$

and plotting the results in Figure 6.4(a). As predicted by the theory presented in theorems 4.3,4.7, these results confirm that the sequence of approximate means form a Cauchy sequence, and hence converge to a limit as the mesh is refined. Similar convergence results were also observed for the means of the other conserved variables, namely momentum and total energy.

Next, we compute the sample variance and show the results in Figure 6.5. The results suggest that the variance also converges with grid resolution. This convergence is also demonstrated quantitatively by plotting the L^1 differences of the variance at successive levels of resolution, shown in Figure 6.4(b). Again, the figure suggests that the sequence forms a Cauchy sequence, and hence is convergent. Furthermore, the variance itself shows no small scale features, even on very fine mesh resolutions (see Figure 6.5). This figure also reveals that the variance is higher near the initial mixing layer.

6.1.3 Strong convergence to an EMV solution

Convergence of the mean and variance (as well as higher moments) confirm the narrow convergence predicted by (the multi-dimensional version of) theorems 4.2,4.7. Note that the convergence illustrated in Figure 6.4 is in L^1 of space-time. Next, we test strong convergence of the numerical approximations by computing the Wasserstein distance between two successive mesh resolutions:

$$W_1 \left(\nu_{(x,t)}^{\Delta x}, \nu_{(x,t)}^{\Delta x/2} \right) \quad (6.4)$$

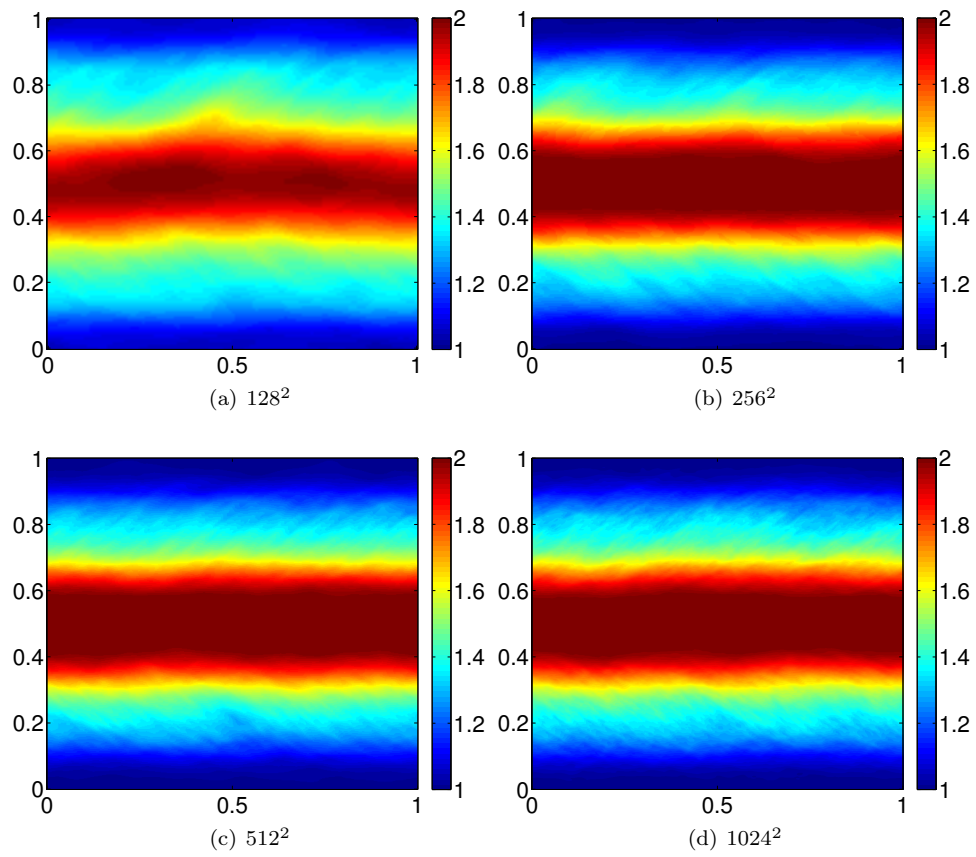


Figure 6.3: Approximate sample means of the density for the Kelvin-Helmholtz problem (6.2) at time $t = 2$ and different mesh resolutions. All results are with 400 Monte Carlo samples.

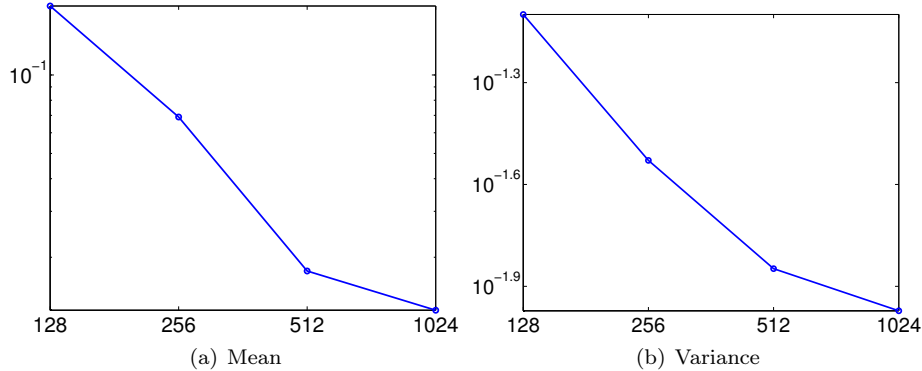


Figure 6.4: Cauchy rates (6.3) for the sample mean and variance of the density (y-axis) vs. mesh resolution (x-axis) for the Kelvin-Helmholtz problem (6.2).

(see Appendix A.1.4). In Figure 6.6 we show the Wasserstein distance between successive mesh resolutions

$$\left\| W_1 \left(\nu_{(\cdot,t)}^{\Delta x}, \nu_{(\cdot,t)}^{\Delta x/2} \right) \right\|_{L^1([0,1]^2)} \quad (6.5)$$

at time $t = 2$. The figure suggests that this difference between successive mesh resolutions converges to zero. Hence, the approximate Young measures converge strongly in both space-time as well as phase space to the limit Young measure.

In Figure 6.7 we show the pointwise difference in Wasserstein distance (6.5) between two successive mesh levels. The figure reveals that this distance decreases as the mesh is refined. Moreover, we see that the Wasserstein distance between approximate Young measures at successive resolutions is concentrated at the interface mixing layers. This is to be expected as the variance is also concentrated along these layers (cf. the variance plots in Figure 6.5).

6.2 Kelvin-Helmholtz: vanishing variance around atomic initial data ($\varepsilon \downarrow 0$)

Our aim is to compute the entropy measure-valued solutions of the two-dimensional Euler equations with atomic initial measure, concentrated on the Kelvin-Helmholtz data (1.8). We utilize Algorithm 4.6 for this purpose and consider the perturbed initial data (6.2). Observe that this perturbed initial data converges strongly to the initial data (1.8) as $\varepsilon \rightarrow 0$. We wish to study the limit behavior of approximate solutions $\nu^{\Delta x, \varepsilon}$ as $\varepsilon \rightarrow 0$. To this end, we compute approximate solutions using the TeCNO2 scheme at a very fine mesh resolution of 1024^2 points for different values of ε .

Results for a single sample at time $t = 2$ and different ε 's are presented in Figure 6.8. The figures indicate that there is no convergence as $\varepsilon \rightarrow 0$. The spread of the mixing region seems to remain large even when the perturbation parameter is reduced. This lack of convergence is further quantified in Figure 6.9, where we plot the L^1 difference of the approximate density for successively reduced values of ε . This difference remains large even when ε is reduced by an order of magnitude.

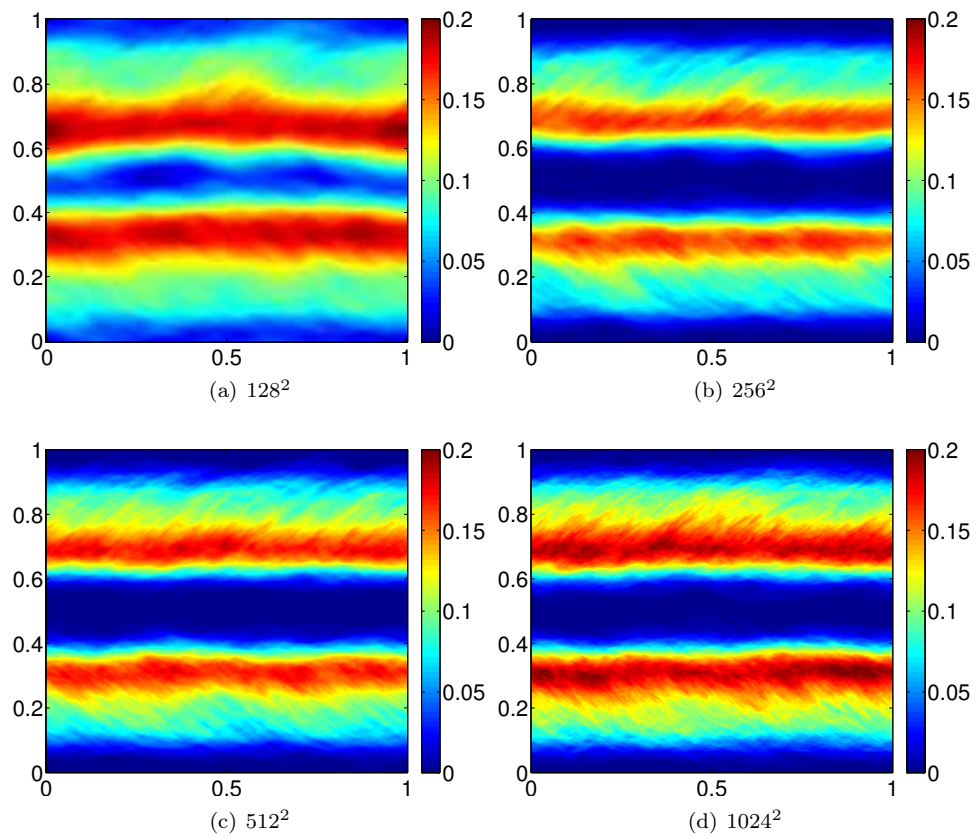


Figure 6.5: Approximate sample variances of the density for the Kelvin-Helmholtz problem (6.2) at time $t = 2$ and different mesh resolutions. All results are with 400 Monte Carlo samples.

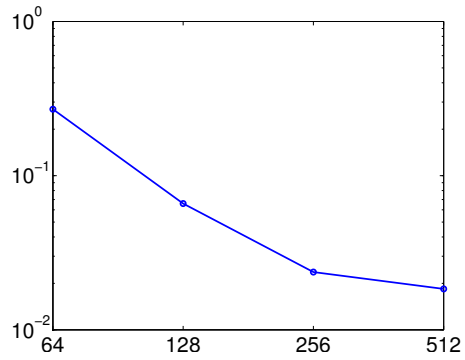


Figure 6.6: Cauchy rates in the Wasserstein distance (6.5) at time $t = 2$ for the density (y-axis) with respect to different mesh resolutions (x-axis), for the Kelvin-Helmholtz problem (6.2).

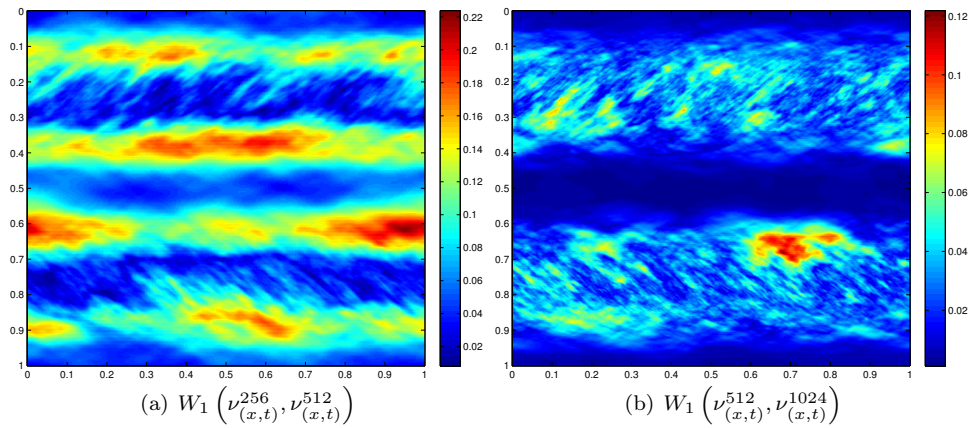


Figure 6.7: Wasserstein distances between the approximate Young measure (density) (6.4) at successive mesh resolutions, at time $t = 2$.

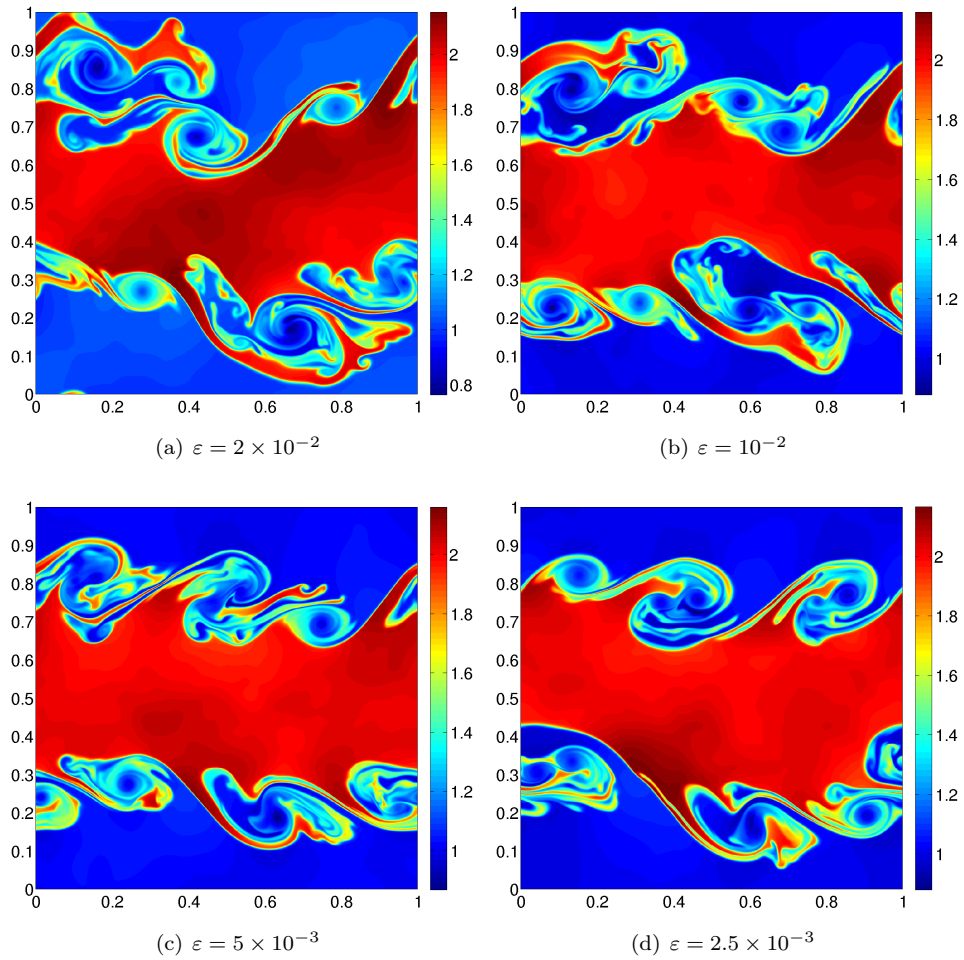


Figure 6.8: Approximate density, computed with the TeCNO2 scheme for a single sample with initial data (6.2) for different initial perturbation amplitudes ε on a grid of 1024^2 points.

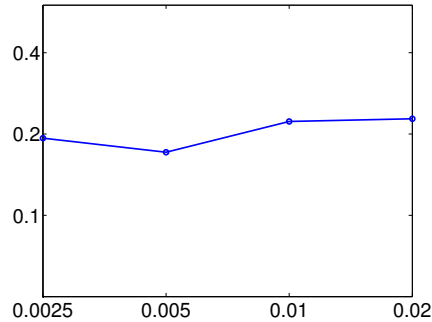


Figure 6.9: The Cauchy rates (L^1 difference for successively reduced ε) for the density (y-axis) at $t = 2$ for a single sample vs. different values of the perturbation parameter ε (x-axis).

Next, we compute the mean of the density over 400 samples at a fixed grid resolution of 1024^2 points and for different values of the perturbation parameter ε . This sample mean is plotted in Figure 6.10. The figure clearly shows pointwise convergence as $\varepsilon \rightarrow 0$, to a limit different from the steady state solution (1.8). This convergence of the mean with respect to decaying ε is quantified in Figure 6.11(a), where we compute the L^1 difference of the mean for successive values of ε . We observe that the mean forms a Cauchy sequence, and hence converges.

Similarly the computations of the sample variance for different values of ε are presented in Figure 6.12. Note that this figure, as well as the computations of the difference in variance in L^1 for successive reductions of the perturbation parameter ε (shown in Figure 6.11(b)), clearly show convergence of variance as $\varepsilon \rightarrow 0$. Moreover, Figure 6.12 clearly indicates that the limit of the variance is non-zero. Hence, this strongly suggests the fact that EMV solution can be non-atomic, even for atomic initial data. These results are consistent with Theorem 4.7.

To further demonstrate the non-atomicity of the resulting measure valued solution, we have plotted the probability density functions for density at the points $x = (0.5, 0.7)$ and $x = (0.5, 0.8)$, in figure 6.13 for a fixed mesh of size 1024^2 . We see that the initial unit mass centered at $\rho = 2$ ($\rho = 1$, respectively) at $t = 0$ is smeared out over time, and at $t = 2$ the mass has spread out over a range of values of ρ between 1 and 2.

Figure 6.14 shows the same quantities, but for a fixed time $t = 2$ over a series of meshes. Although a certain amount of noise seems to persist on the finer meshes – most likely due to the low number of Monte Carlo samples – it can be seen that the probability density functions seem to converge with mesh refinement.

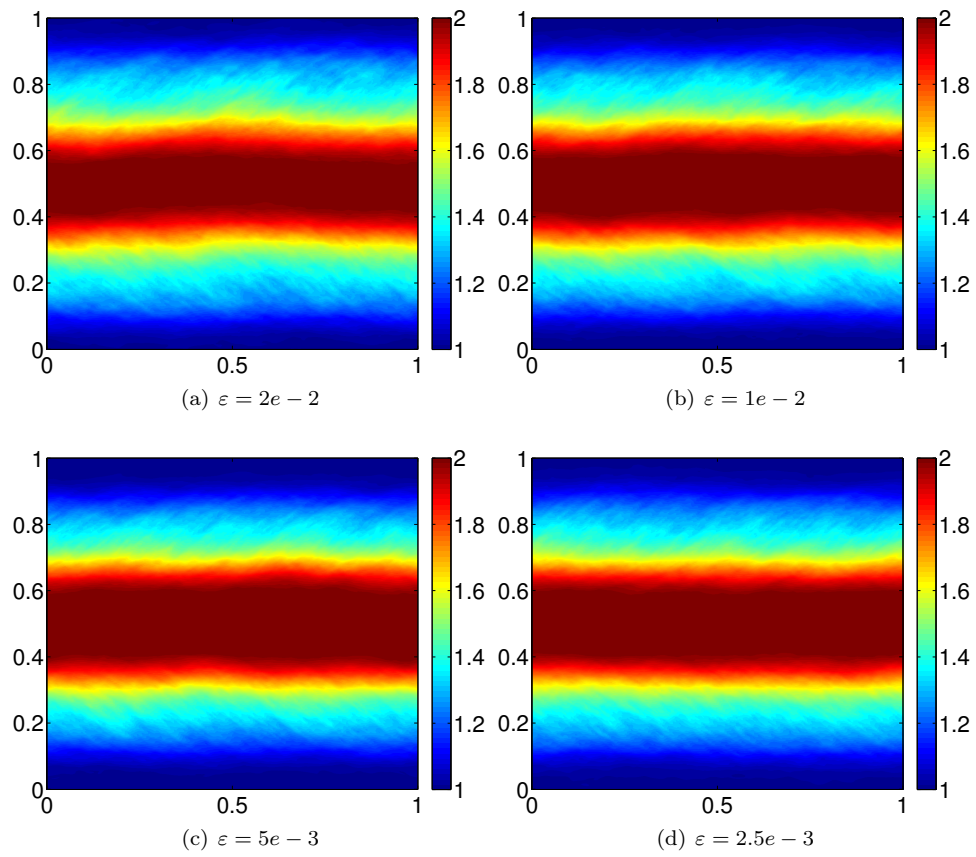


Figure 6.10: Approximate sample means of the density for the Kelvin-Helmholtz problem (6.2) at time $t = 2$ and different values of perturbation parameter ε . All the computations are on a grid of 1024^2 mesh points and 400 Monte-Carlo samples.

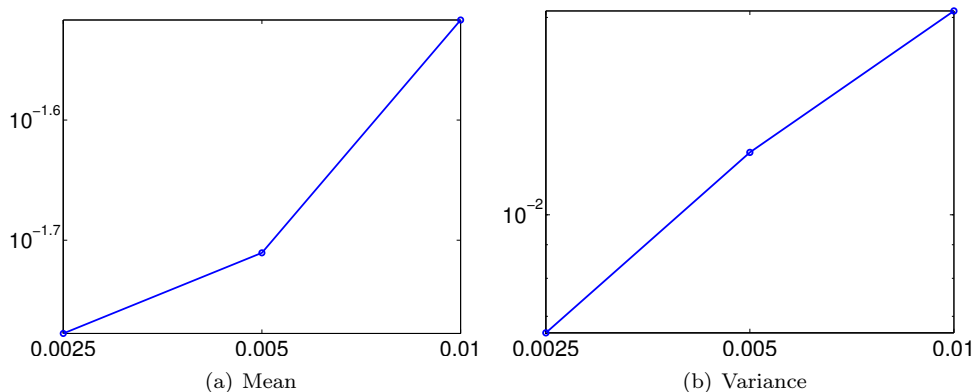


Figure 6.11: Cauchy rates for the sample mean and the sample variance of the density (y-axis) for the Kelvin-Helmholtz problem (6.2) for different values of ε (x-axis). All the computations are on a grid of 1024^2 mesh points and 400 Monte-Carlo samples.

6.3 Richtmeyer-Meshkov problem

As a second numerical example, we consider the two-dimensional version of the Euler equations (6.1) in the computational domain $x \in [0, 1]^2$ with initial data:

$$p(x) = \begin{cases} 20 & \text{if } |x| < 0.1 \\ 1 & \text{otherwise,} \end{cases} \quad \rho(x) = \begin{cases} 2 & \text{if } |x| < I(x, \omega) \\ 1 & \text{otherwise,} \end{cases} \quad w^x = w^y = 0. \quad (6.6)$$

The radial density interface $I(x, \omega) = 0.25 + \varepsilon Y(\varphi(x), \omega)$ is perturbed with

$$Y(\varphi, \omega) = \sum_{n=1}^m a^n(\omega) \cos(\varphi + b^n(\omega)), \quad (6.7)$$

where $\varphi(x)$ is the angle of x with the positive x_1 -axis, and a_n, b_n, k are the same as in Section 6.1.

6.3.1 Lack of sample convergence

As in the case of the Kelvin-Helmholtz problem, we test whether numerical approximations for a single sample converge as the mesh is refined. To this end, we compute the approximations of the two-dimensional Euler equations with initial data (6.6) using a second-order finite volume scheme implemented in the FISH code [42]. The numerical results, presented in Figure 6.15, show the effect of grid refinement on the density for a single sample at time $t = 4$. As seen from this figure, there seems to be no convergence as the mesh is refined. This lack of convergence is quantified in Figure 6.16, where we present differences in L^1 for successive mesh resolutions (1.7) and see that the approximate solutions for a single sample do not form a Cauchy sequence.

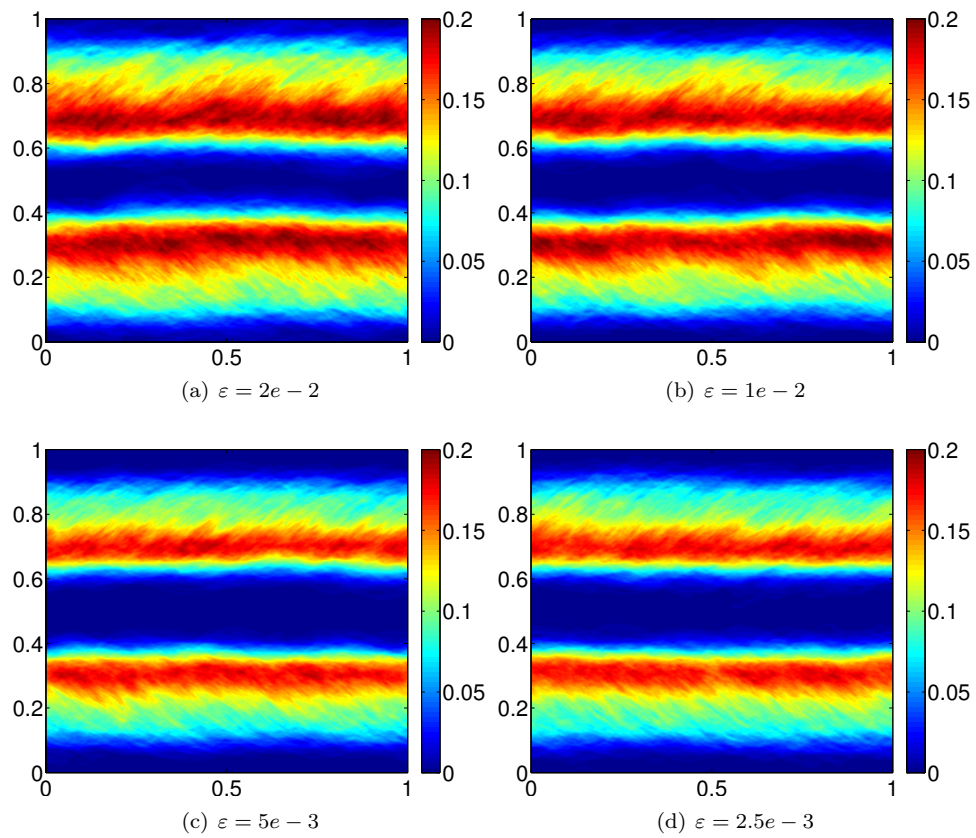


Figure 6.12: Approximate sample variances of the density for the Kelvin-Helmholtz instability at time $t = 2$ and different values of perturbation parameter ε . All the computations are on a grid of 1024^2 mesh points and 400 Monte-Carlo samples

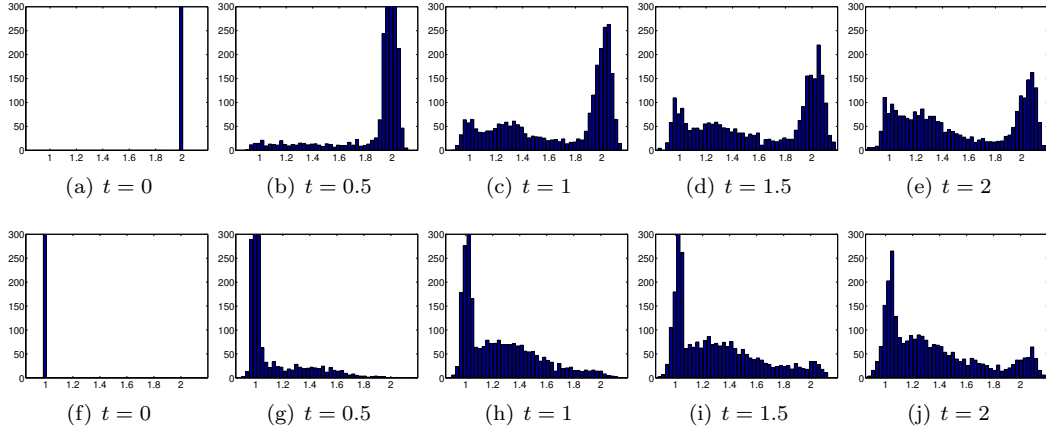


Figure 6.13: The approximate PDF for density ρ at the points $x = (0.5, 0.7)$ (first row) and $x = (0.5, 0.8)$ (second row) on a grid of 1024^2 mesh points.

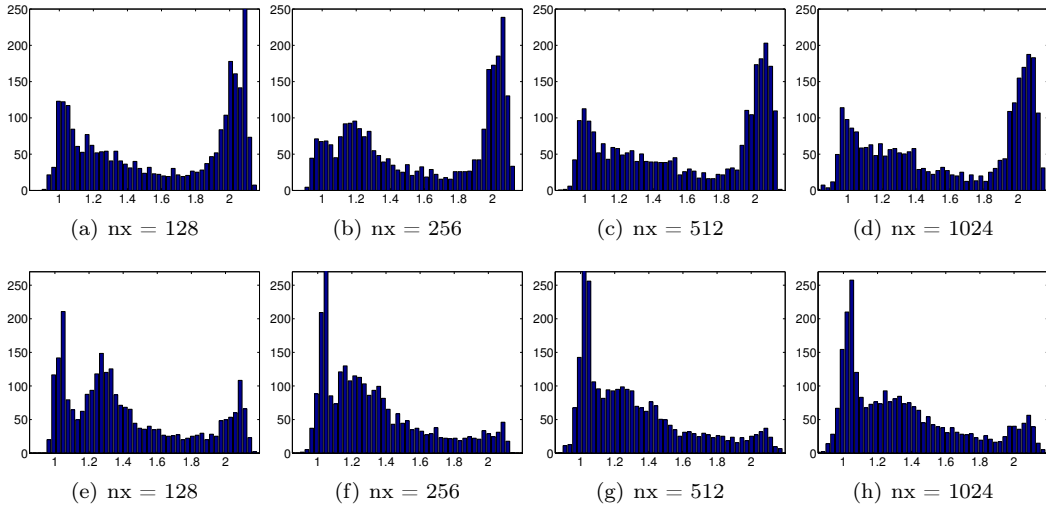


Figure 6.14: The approximate PDF for density ρ at the points $x = (0.5, 0.7)$ (first row) and $x = (0.5, 0.8)$ (second row) a series of meshes.

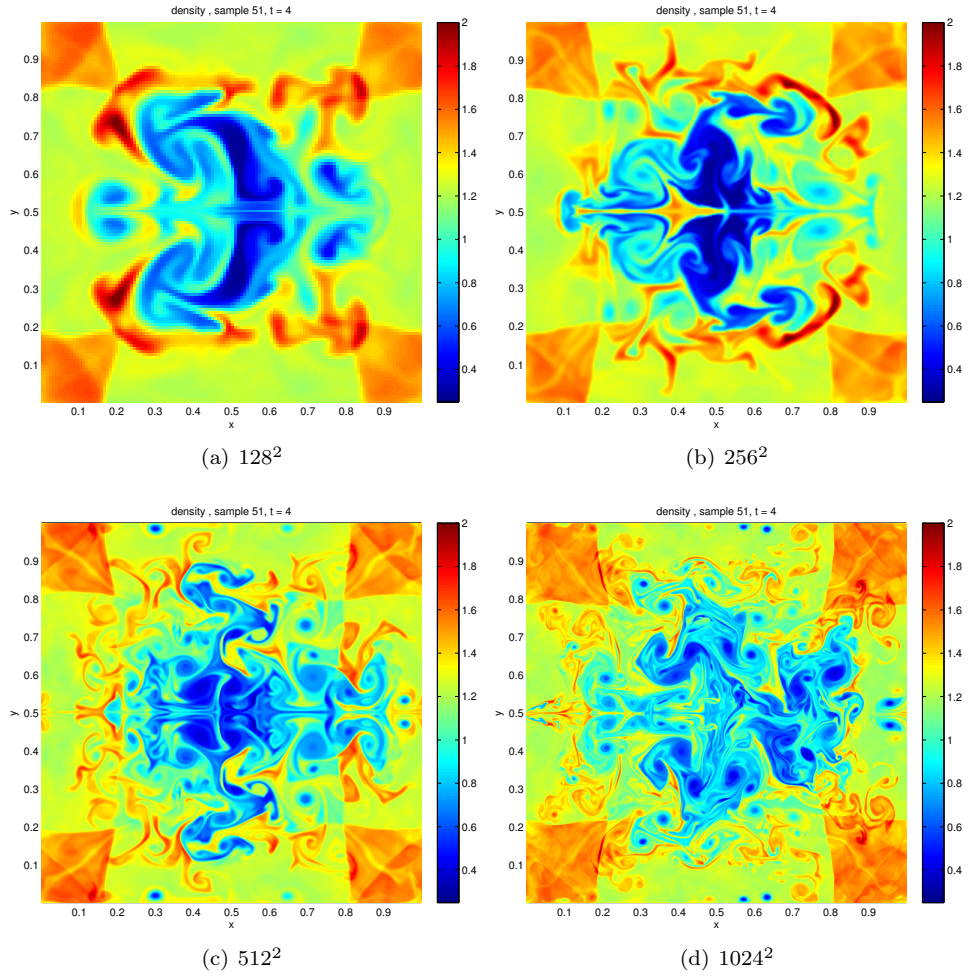


Figure 6.15: Approximate density for a single sample for the Richtmyer-Meshkov problem (6.6) for different grid resolutions at time $t = 4$.

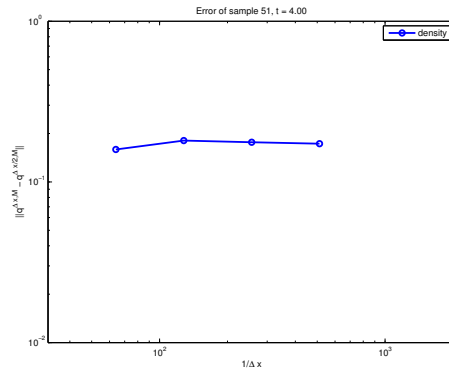


Figure 6.16: Cauchy rates (1.7) for the density (y-axis) in a single sample of the Richtmeyer-Meshkov problem (6.6) at time $t = 4$, with respect to different grid resolutions (x-axis).

6.3.2 Convergence of the mean and the variance

Next, we test for convergence of statistical quantities of interest as the mesh is refined. First, we check the convergence of the mean through the Monte Carlo approximation (4.9) with $M = 400$ samples. The numerical results for the density at time $t = 4$ at different grid resolutions are presented in Figure 6.17. The figure clearly shows that the mean converges as the mesh is refined. This convergence is further verified in Figure 6.18(a) where we plot the difference in mean (6.3) for successive resolutions. This figure proves that the mean of the approximations form a Cauchy sequence and hence, converge. From Figure 6.17, we also observe that small scale features are averaged out in the mean and only large scale structures, such as the strong shocks and mixing regions, are retained through the averaging process.

Next, we check for the convergence of the variance for the Richtmeyer-Meshkov problem (6.6). The results, shown in Figure 6.19 for time $t = 4$, at different mesh resolutions and with 400 Monte Carlo approximations, clearly indicate that the variance of the approximate Young measures converge as the mesh is refined. This is also verified from Figure 6.18(b) where the difference in L^1 of the variances at successive mesh resolutions is plotted and shown to form a Cauchy sequence.

6.4 Measure valued (MV) stability

The above experiments clearly illustrate that the numerical procedure proposed here does succeed in computing an EMV solution of the underlying systems of conservation laws (2.3). Are the computed solutions stable?. As argued in Section 3, uniqueness (stability) of EMV solutions for a general MV initial data is not necessarily true, even for scalar conservation laws. Moreover, the scalar case suggests that at most a weaker concept of stability, that of MV stability can be expected for EMV solutions (see Terminology 3.4). As stated before, MV stability amounts to stability with respect to perturbations of atomic initial data. We examine this weaker notion of stability through numerical experiments.

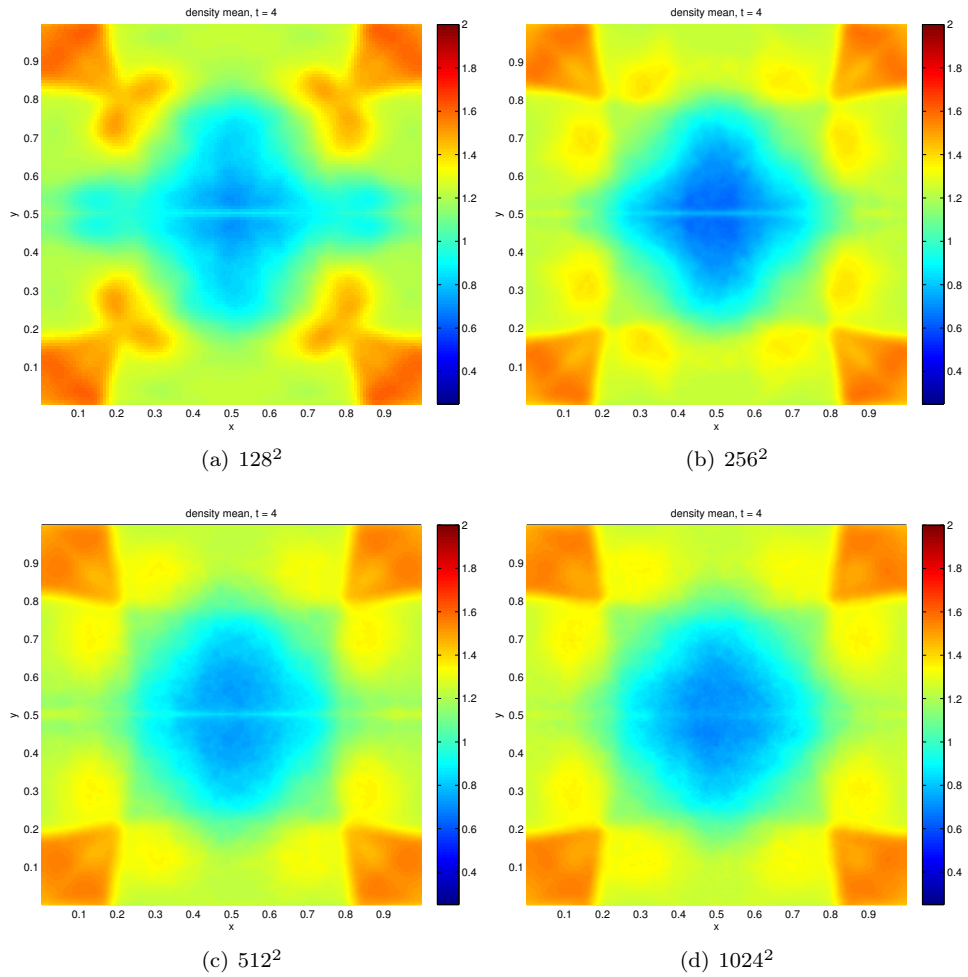


Figure 6.17: The mean density for the Richtmeyer-Meshkov problem with initial data (6.6) for different grid resolutions at time $t = 4$. All results are obtained with 400 Monte Carlo samples.

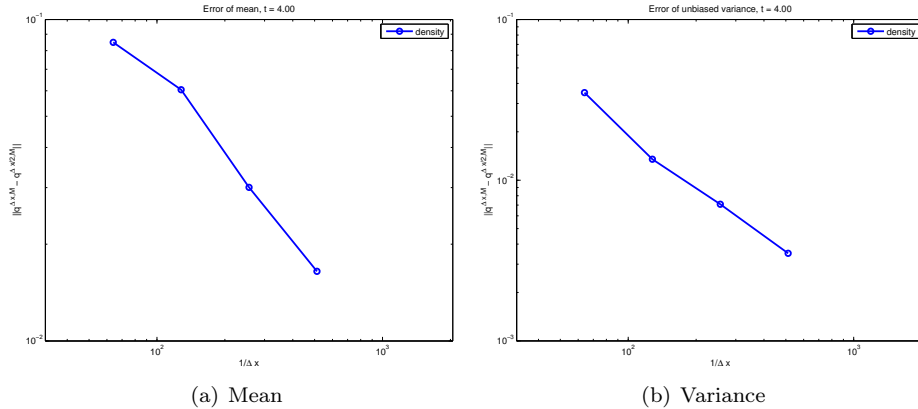


Figure 6.18: Cauchy rates (6.3) for the mean and variance (y-axis) of the Richtmyer-Meshkov problem (6.6) at time $t = 4$ and at different grid resolutions (x-axis). All results are obtained with 400 Monte Carlo samples.

To this end, we consider the Kelvin-Helmholtz problem as our test bed and investigate stability with respect to the following perturbations:

6.4.1 Stability with respect to different numerical schemes.

As a first check of MV stability, we consider the perturbed Kelvin-Helmholtz initial data (6.2) with a fixed perturbation size $\varepsilon = 0.01$ and compute approximate measure valued solutions using Algorithm 4.1. Three different schemes are compared:

1. (Formally) second-order TeCNO2 scheme [25].
2. Third-order TeCNO3 scheme [25].
3. Second-order high-resolution finite volume scheme, based on the HLLC approximate Riemann solver, and implemented in the FISH code [42].

We will compare the mean and the variance of the approximate measures, at a resolution of 1024^2 points and 400 Monte Carlo samples, at time $t = 2$. As the mean and the variance with TeCNO2 scheme have already been depicted in Figures 6.3(d) and 6.5(d), respectively, we plot the mean and variance with the TeCNO3 and FISH schemes in Figure 6.20. These results, together with the results for the TeCNO2 scheme (Figures 6.3(d) and 6.5(d)) clearly show that mean and variance of the approximate measure valued solution are very similar even though the underlying approximation schemes are different. In particular, comparing the TeCNO2 and TeCNO3 schemes, we observe that although both schemes have the same design philosophy (see [25] and section 5), their formal order of accuracy is different. Hence, the underlying numerical viscosity operators are different. In spite of different numerical regularizations, both schemes seem to be converging to the same measure valued solution – at least in terms of its first and second moments. This agreement is even more surprising

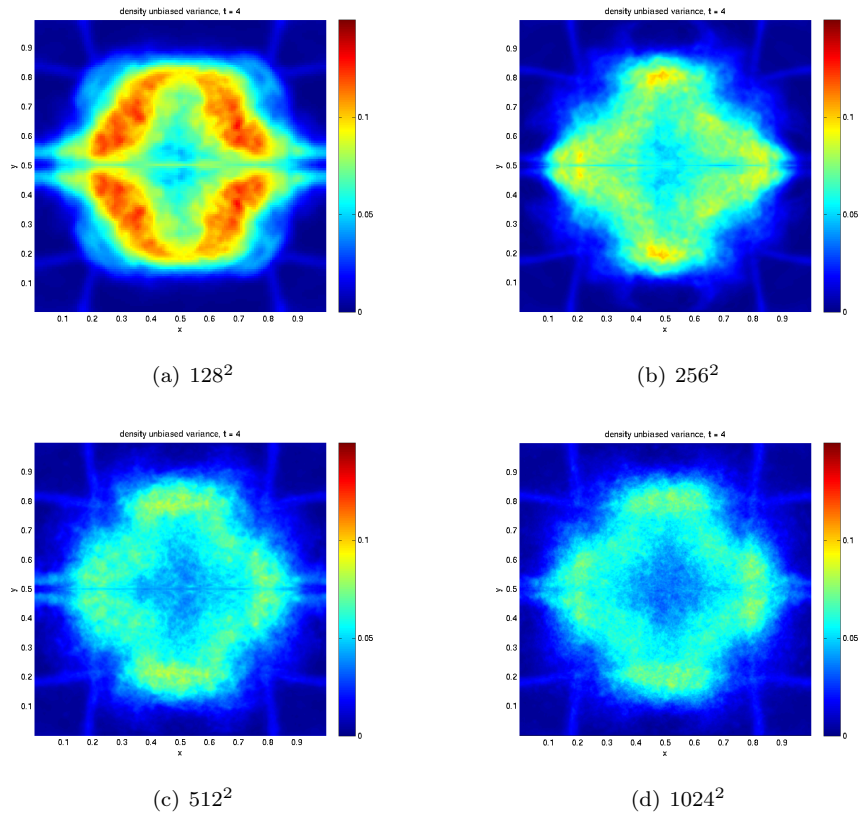


Figure 6.19: Variance of the density with initial data (6.6) for different grid resolutions at time $t = 4$. All results are obtained with 400 Monte Carlo samples.

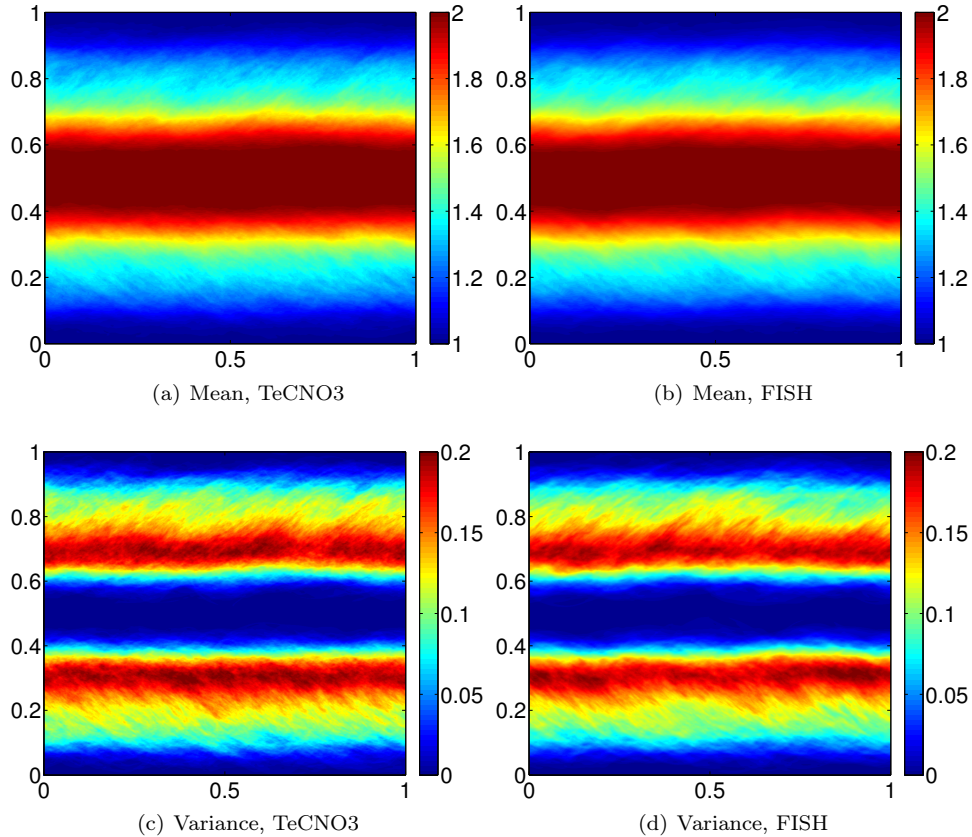


Figure 6.20: Mean and variance of the density for the Kelvin-Helmholtz problem with initial data (6.2), at time $t = 2$ at a resolution of 1024^2 points and with 200 Monte Carlo samples. Different numerical schemes are compared.

for the FISH scheme of [42]. This scheme utilizes a very different design philosophy based on HLLC approximate Riemann solvers and an MC slope limiter. Furthermore, it is unclear whether this particular scheme satisfies the discrete entropy inequality (4.6) or the weak BV bound (4.5). Nevertheless, the measure valued solutions computed by this scheme seem to converge to the same EMV solution as computed by the TeCNO schemes. We have observed similar agreement between different schemes for smaller values of the perturbation parameter ε as well as in the Richtmeyer-Meshkov problem. These numerical results at least indicate MV stability with respect to different numerical discretizations.

6.4.2 MV stability with respect to different perturbations

A more stringent test of MV stability is with respect to different types of initial perturbations. To be more specific, we consider the Kelvin-Helmholtz problem with the phase perturbations

of (6.2) and compare them with amplitude perturbations (1.5) and (1.8). Note that for small values of the perturbation parameter ε , both the amplitude and phase perturbations are close to the atomic initial data (1.8) and to one another (for instance in the Wasserstein metric). We test whether the resulting approximate MV solutions are also close. To this end, we compute the approximate measure valued solutions with the phase perturbation and amplitude perturbation, for $\varepsilon = 0.0005$, with the TeCNO3 scheme, at a grid resolution of 1024^2 points and 400 Monte Carlo samples, and plot the results in Figure 6.21. The results show that the mean and variance with different initial perturbations are very similar when the amplitude ε of the perturbations is small.

A further stringent test of stability is provided by the following phase perturbation of the Kelvin-Helmholtz problem (6.2). The same set-up as in the description of (6.2) is used but with an interface perturbation of the form:

$$I_j = I_j(x_1, \omega) := J_j + \varepsilon Y_j(x_1, \omega). \quad (6.8)$$

As in (6.2), we set $J_1 = 0.25$ and $J_2 = 0.75$ but with an interface variation of the form:

$$Y_j(x_1, \omega) = \sum_{n=1}^k a_j^n \mathbb{1}_{A_n}, \quad j = 1, 2. \quad (6.9)$$

Here, $a_j^n = a_j^n(\omega) \in [-1/2, 1/2]$ are randomly chosen numbers from a uniform distribution. As a second variant, the a_j^n are drawn from the standard normal distribution. The A_n are equally spaced intervals, i.e. $A_n = [(n-1)h, nh)$ with $h = 1/32$. Thus, the initial interface perturbation is discontinuous, with uncorrelated random variation of the interface inside each interval. Such types of random initial data are motivated from observed or measured data, see [53].

The resulting approximate MV solutions, computed with a perturbation of size $\varepsilon = 0.005$, at time $t = 2$ and at a resolution of 1024^2 are shown in Figure 6.22. The mean (top) and variance (bottom) are plotted. Results with the coefficients a_j^n , chosen from both an uniform distribution (left) as well as a standard normal distribution (right) are shown. As seen from the figure, the computed mean and variance appear identical to each other. Furthermore, they are very similar to the mean and variance computed with the amplitude perturbation (1.5) and (1.8) as well as the sinusoidal phase perturbation (6.2) (compare with Figure 6.21). Thus, we observe that the computed MV solutions are very similar to each other, even for four different sets of initial perturbations. This clearly indicates MV stability of the computed MV solution with the Kelvin-Helmholtz initial data.

7 Discussion

We conclude with a brief discussion on the highlights of the current paper which are put in perspective for future results. Currently, the notion of entropy solutions is the most widely accepted solution framework for systems of hyperbolic conservation laws (1.1). Entropy solutions are bounded functions which satisfy the equation in the sense of distributions (1.2) and also satisfy an entropy inequality (1.3). Although the existence and uniqueness of entropy solutions has been established for multi-dimensional scalar conservation laws and for one-dimensional systems, there are no known global existence and uniqueness (stability)

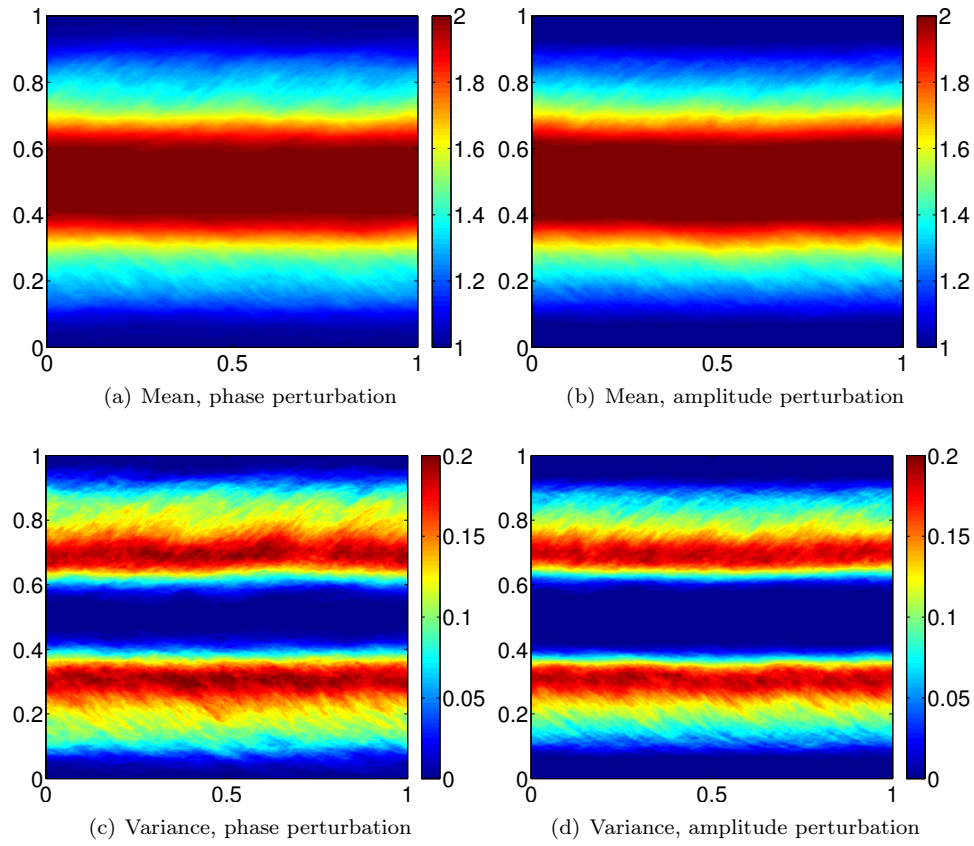


Figure 6.21: Mean (Top) and variance (bottom) of the density for the Kelvin-Helmholtz problem with different initial data: phase perturbations (6.2) (Left) and amplitude perturbations (1.8), (1.5) (Right), at time $t = 2$ at a resolution of 1024^2 points and with 400 Monte Carlo samples. All computations are with the TeCNO3 scheme.

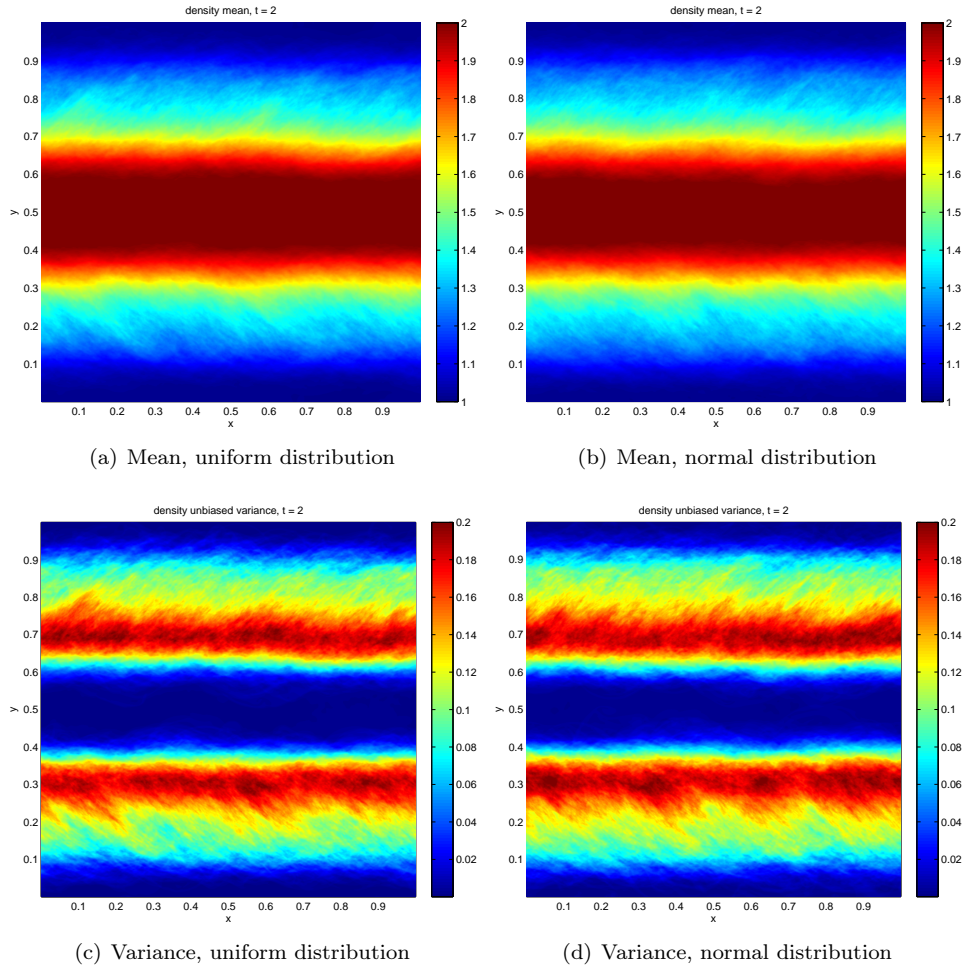


Figure 6.22: Mean (Top) and variance (bottom) of the density for the Kelvin-Helmholtz problem with different initial data: discontinuous phase perturbations (6.8) with uniformly distributed coefficients in (6.9) (Left) and with (standard) normally distributed coefficients in (6.9) (Right), at time $t = 2$ at a resolution of 1024^2 points and with 400 Monte Carlo samples. All computations are with the second-order FISH scheme.

results for generic multi-dimensional systems. In fact, recent papers [18, 19] provides examples of multi-dimensional systems with infinitely many entropy solutions.

Although a wide variety of numerical methods, such as finite volume, finite difference and discontinuous Galerkin methods have been developed and successfully employed to approximate systems of conservation laws, none of these methods has been shown to converge to an entropy solution for a generic system of conservation laws.

Numerical evidence – lack of convergence for weak solutions. In the current paper we present numerical experiments to demonstrate that even state of the art numerical methods may not necessarily converge as the mesh is refined. As shown in Figures 1.3 and 6.1, finer and finer structures emerge as the grid is refined. This generation of oscillations at finer and finer scales prevents convergence under mesh refinement. We also present numerical experiments that demonstrate the lack of stability of entropy solutions with respect to perturbations of initial data; see Figures 1.4(b) and 6.8.

This lack of convergence of numerical methods, coupled with recent results on non-uniqueness of entropy solutions, motivates us to seek a more general, weaker notion of solutions for systems of conservation laws. To this end, we focus on the notion of entropy measure-valued (EMV) solutions, first introduced by DiPerna in [22], see also [23]. We propose a measure-valued Cauchy problem (2.3) by allowing the initial data to be a Young measure – a parametrized probability measure. The sought-for solution is a Young measure that is consistent with the underlying equations in the sense of distributions (2.4) and satisfies a suitable form of the entropy inequality (2.5). The consideration of general measure-valued data also allows us to incorporate initial uncertainty and to encompass various formalisms for uncertainty quantification for conservation laws.

The main aim of the current paper was to design numerical methods that can be rigorously shown to converge to an EMV solution. We work with an equivalent representation of measures as probability laws of random fields. The initial random field is then evolved using a numerical scheme. The law of the resulting (random) narrowly convergent approximations provides an approximation to the measure valued solution. For a numerical scheme to be narrowly convergent, it is required to satisfy a set of minimal criteria outlined in Theorem 4.2:

- Uniform boundedness of the approximations in L^∞ ;
- Discrete entropy inequality;
- Space-time weak BV bound.

The TeCNO schemes of [25] and the space-time DG schemes of [38] are examples of (formally) high-order schemes satisfying the discrete entropy inequality and weak BV bounds. The uniform L^∞ bound is a technical assumption that will be relaxed in a forthcoming paper [27].

Thus, we provide sufficient conditions that can guide the design of numerical methods for systems of conservation laws. Note that for systems of conservation laws, the above conditions play a role similar to that played by the well-known criteria of discrete maximum principles, entropy inequalities and the TVD property in the numerical analysis of scalar conservation laws.

The convergence of numerical approximations to an EMV solution of (2.3) is interpreted the narrow sense, meaning that statistics of space-time averages of the unknowns converge as the mesh is refined. These statistical quantities require computation of integrals over phase space. A Monte Carlo approximation is used to compute these phase space integrals and show convergence of the resulting numerical procedure. This, to our knowledge, provides a first set of rigorous convergence results for numerical approximations of generic multi-dimensional systems of conservation laws.

What do our numerical experiments tell us. A large number of numerical experiments illustrating the convergence theory are presented. The key observations from the numerical experiments are as follows.

- In general, there is no observed convergence of numerical approximations (in L^1 as well as even weaker norms) for single realizations (samples), with respect to increasing mesh resolutions. This has been demonstrated with two examples for the two-dimensional Euler equations.
- However, as predicted by the theory, statistical quantities of interest such as the mean and the variance of an ensemble of solutions do converge as the mesh is refined.
- In fact, a stronger convergence is observed. The approximate Young measures seem to converge in the strong sense (2.2) to an EMV solution.

The numerical approximation procedure, presented in Algorithm 4.5, was also employed to compute EMV solutions with respect to atomic initial data. In general, the resulting measure valued solution is not atomic, see Figures 6.12, 6.13 and 6.14. This key observation implies that the nonlinearity in the conservation law acts to spread the support of the initial atomic measure. This bursting out of the initial atomic measure is, in our opinion, as significant as the formation of shock waves in nonlinear conservation laws. Formation of shock waves precludes the existence of global classical solutions, even for scalar conservation laws. Similarly, the bursting out of initial atomic measures implies that we have to look beyond integrable functions in order to obtain existence of solutions to systems of conservation laws. The concept of entropy measure-valued solutions appears to be a natural extension. The numerical results presented in this paper do indicate closure within this class of solutions. Stability. As the results of this paper and the forthcoming paper [27] show, the convergence of numerical approximations also provides a (constructive) proof of existence for EMV solutions of (2.3). The questions of uniqueness and stability are more delicate. From Example 3.2 and the results of [57] and references therein, we know that EMV solutions may not be unique if the initial measure is non-atomic, even for scalar conservation laws. We propose a weaker stability concept, that of measure-valued stability. This concept implies stability for statistics of space-time averages in problems where the initial measure is close to atomic. Numerical experiments examining this weaker concept of stability were presented in section 6.4. From these experiments, we observed that

- Different numerical schemes appear to converge to the same EMV solution as the mesh is refined.
- Different types of perturbations of atomic initial data were considered and the resulting approximate EMV solutions seemed to converge to the same EMV solution, corresponding to atomic initial data.

These experiments indicate that our approximation procedure is indeed stable. Furthermore, they also suggest that the weaker notion of MV stability might be an appropriate framework to discuss the question of stability of EMV solutions.

However, the only rigorous results that we obtain are of the measure valued-strong uniqueness type, see Theorem 3.5 and [9, 20]. Here, the stability is ensured when a classical solution (an atomic measure concentrated on a Lipschitz solution) is present. This also implies local (in time) uniqueness of EMV solutions for atomic initial data, concentrated on smooth functions. Given the paucity of rigorous stability results, there is a considerable scope for the theoretical investigation of weaker concepts of stability, such as measure valued stability for systems of conservation laws. Moreover, additional admissibility criteria such as entropy rate criteria of [17] or other variants might be necessary to ensure even MV stability of the EMV solution.

Narrowly convergent schemes. As mentioned before, we have provided a numerical procedure, as well as sufficient conditions on numerical schemes, such that the approximations converge to an EMV solution. Some examples of schemes satisfying these criteria were presented. These results will hopefully encourage the development of other kinds of numerical schemes, such as of the WENO, RKDG and spectral viscosity type, that satisfy the abstract criteria of this paper, and hence converge to measure valued solutions of systems of conservation laws.

Computing the measure valued solution requires evaluation of phase space integrals. Our proposal in this paper was to employ Monte Carlo sampling. This procedure can be very expensive computationally, on account of the slow convergence with respect to the number of samples. We foresee the design of more computationally efficient methods by adapting schemes such as Multi-level Monte Carlo [51, 52, 53], stochastic collocation finite volume methods [54] and gPC based stochastic Galerkin methods [21], which have recently been developed to deal with uncertainty quantification for systems of conservation laws. Such extensions are the subject of ongoing research.

A Young measures

We provide here a very short introduction to Young measures. The reader may wish to consult [28, 8] for the theory of Radon measures and probability measures, and [4, 3] on the theory of Young measures.

A.1 Probability measures

A.1.1 We denote by $\mathcal{M}(\mathbb{R}^N)$ the set of finite Radon measures on \mathbb{R}^N , which are inner regular Borel measures μ with finite total variation $|\mu|(\mathbb{R}^N)$. Let $C_0(\mathbb{R}^N)$ be the space of continuous real-valued functions on \mathbb{R}^N which vanish at infinity, equipped with the supremum norm. Then it can be shown (see e.g. [28, Section 7.3]) that $\mathcal{M}(\mathbb{R}^N)$ can be identified with the dual space of $C_0(\mathbb{R}^N)$ through the pairing $\langle \mu, g \rangle = \int_{\mathbb{R}^N} g(\xi) d\mu(\xi)$. We do not distinguish between these two equivalent definitions of \mathcal{M} . By a slight abuse of notation, we shall sometimes write $\langle \mu, g(\xi) \rangle = \int_{\mathbb{R}^N} g(\xi) d\mu(\xi)$. We will be particularly interested in the pairing $\langle \mu, \text{id} \rangle = \int_{\mathbb{R}^N} \xi d\mu(\xi)$ between μ and the identity function $\text{id}(\xi) = \xi$.

A.1.2 The duality between $C_0(\mathbb{R}^N)$ and $\mathcal{M}(\mathbb{R}^N)$ induces a weak* topology on $\mathcal{M}(\mathbb{R}^N)$, that of narrow convergence. A sequence $\mu^n \in \mathcal{M}(\mathbb{R}^N)$ converges narrowly to $\mu \in \mathcal{M}(\mathbb{R}^N)$ provided $\langle \mu^n, g \rangle \rightarrow \langle \mu, g \rangle$ for all $g \in C_0(\mathbb{R}^N)$. (This is also called weak or weak* convergence, see [8].)

A.1.3 The set of probability measures on \mathbb{R}^N is the subset

$$\mathcal{P}(\mathbb{R}^N) := \{ \mu \in \mathcal{M}(\mathbb{R}^N) : \mu \geq 0, \mu(\mathbb{R}^N) = 1 \}.$$

Let $\mathcal{P}^p(\mathbb{R}^N) \subset \mathcal{P}(\mathbb{R}^N)$ for $p \in [1, \infty)$ denote the set of probability measures μ such that $\langle \mu, |\xi|^p \rangle < \infty$. For $\mu, \rho \in \mathcal{P}^p(\mathbb{R}^N)$ the Wasserstein metric W_p is defined as

$$W_p(\mu, \rho) := \inf \left\{ \int_{\mathbb{R}^N \times \mathbb{R}^N} |\xi - \zeta|^p d\pi(\xi, \zeta) : \pi \in \Pi(\mu, \rho) \right\}^{1/p},$$

where $\Pi(\mu, \rho)$ is the set of probability measures on $\mathbb{R}^N \times \mathbb{R}^N$ with marginals μ and ρ :

$$\Pi(\mu, \rho) := \left\{ \pi \in \mathcal{P}(\mathbb{R}^N \times \mathbb{R}^N) : \pi(A \times \mathbb{R}^N) = \mu(A), \pi(\mathbb{R}^N \times A) = \rho(A) \forall \text{ Borel } A \subset \mathbb{R}^N \right\}.$$

It can be shown that W_p for any p metrizes the topology of narrow convergence on $\mathcal{P}^p(\mathbb{R}^N)$, see Proposition 7.1.5 in [1].

A.1.4 Let $\mu, \rho \in \mathcal{P}(\mathbb{R})$, and let $F, G : \mathbb{R} \rightarrow [0, 1]$ be their distribution functions,

$$F(x) := \mu((-\infty, x]), \quad G(y) := \rho((-\infty, y]).$$

Then it can be shown that

$$W_p(\mu, \rho) = \left(\int_0^1 |F^{-1}(s) - G^{-1}(s)|^p ds \right)^{1/p},$$

see Major [50, Theorem 8.1]. This gives rise to an efficient algorithm for computing the Wasserstein distance between discrete probability distributions. Let x_1, \dots, x_n and y_1, \dots, y_n be random numbers drawn from the probability distributions μ and ρ , respectively, and define the discrete distributions $\mu_n := (\delta_{x_1} + \dots + \delta_{x_n})/n$ and $\rho_n := (\delta_{y_1} + \dots + \delta_{y_n})/n$. By the law of large numbers, we have $\mu_n \rightarrow \mu$ and $\rho_n \rightarrow \rho$ narrowly as $n \rightarrow \infty$, almost surely. Moreover, their distribution functions are

$$F_n(x) = \frac{\#\{x_j : x_j \leq x\}}{n}, \quad G_n(y) = \frac{\#\{y_j : y_j \leq y\}}{n}.$$

Hence, if the sequences x_j and y_j are sorted in increasing order, then

$$W_p(\mu_n, \rho_n)^p = \int_0^1 |F_n^{-1}(s) - G_n^{-1}(s)|^p ds = \frac{1}{n} \sum_{j=1}^n |x_j - y_j|^p.$$

The latter expression is very easy to implement on a computer.

The analogous problem when $\mu, \rho \in \mathcal{P}(\mathbb{R}^N)$ is more complex, but can be solved in $O(n^3)$ time using the so-called Hungarian algorithm; see [55].

A.2 Young measures

A.2.1 A Young measure from $D \subset \mathbb{R}^k$ to \mathbb{R}^N is a function which maps $z \in D$ to a probability measure on \mathbb{R}^N . More precisely, a Young measure is a weak* measurable map $\nu : D \rightarrow \mathcal{P}(\mathbb{R}^N)$, that is, the mapping $z \mapsto \langle \nu(z), g \rangle$ is Borel measurable for every $g \in C_0(\mathbb{R}^N)$. We denote the image of $z \in D$ under ν by $\nu_z := \nu(z) \in \mathcal{P}(\mathbb{R}^N)$. The set of all Young measures from D into \mathbb{R}^N is denoted by $\mathbf{Y}(D, \mathbb{R}^N)$. When $N = 1$ we write $\mathbf{Y}(D) := \mathbf{Y}(D, \mathbb{R})$.

A.2.2 A Young measure $\nu \in \mathbf{Y}(D, \mathbb{R}^N)$ is uniformly bounded if there is a compact set $K \subset \mathbb{R}^N$ such that $\text{supp } \nu_z \subset K$ for all $z \in D$. Note that if ν is atomic, $\nu = \delta_u$, then ν is uniformly bounded if and only if $\|u\|_{L^\infty(D)} < \infty$.

A.2.3 If $u : \mathbb{R}^k \rightarrow \mathbb{R}^N$ is any measurable function then $\nu_z := \delta_{u(z)}$ defines a Young measure, and we have $u(z) = \langle \nu_z, \text{id} \rangle$ for every z . Conversely, we will say that a given Young measure ν is atomic if it can be written as $\nu = \delta_u$ for a measurable function u .

A.2.4 Two topologies on $\mathbf{Y}(D, \mathbb{R}^N)$ arise naturally in the study of Young measures: those of narrow and strong convergence. A sequence $\nu^n \in \mathbf{Y}(D, \mathbb{R}^N)$ converges narrowly to $\nu \in \mathbf{Y}(D, \mathbb{R}^N)$ if $\langle \nu^n, g \rangle \xrightarrow{*} \langle \nu, g \rangle$ in $L^\infty(D)$ for all $g \in C_0(\mathbb{R}^N)$, that is,

$$\int_D \varphi(z) \langle \nu_z^n, g \rangle dz \rightarrow \int_D \varphi(z) \langle \nu_z, g \rangle dz \quad \forall \varphi \in L^1(D),$$

see [2]. We say that $\nu^n \in \mathbf{Y}(D, \mathbb{R}^N)$ converges strongly to $\nu \in \mathbf{Y}(D, \mathbb{R}^N)$ if

$$\|W_p(\nu^n, \nu)\|_{L^p(D)} \rightarrow 0$$

for some $p \in [1, \infty)$. If ν is atomic, $\nu = \delta_u$ for some $u : D \rightarrow \mathbb{R}^N$, then $\nu^n \rightarrow \nu$ strongly if and only if

$$\int_D \int_{\mathbb{R}^N} |\xi - u(z)|^p d\nu_z^n(\xi) dz \rightarrow 0.$$

A.2.5 The fundamental theorem of Young measures was first introduced by Tartar for L^∞ -bounded sequences [62] and then generalized by Schonbek [58] and Ball [4] for sequences of measurable functions. We provide a further generalization: every sequence $\nu^n \in \mathbf{Y}(D, \mathbb{R}^N)$ which does not “leak mass at infinity” (condition (A.1)) has a narrowly convergent subsequence:

Theorem A.1. Let $\nu^n \in \mathbf{Y}(D, \mathbb{R}^N)$ for $n \in \mathbb{N}$ be a sequence of Young measures. Then there exists a subsequence ν^m which converges narrowly to a nonnegative measure-valued function $\nu : D \rightarrow \mathcal{M}_+(\mathbb{R}^N)$ in the sense that

(i) $\langle \nu^m, g \rangle \xrightarrow{*} \langle \nu, g \rangle$ in $L^\infty(D)$ for all $g \in C_0(\mathbb{R}^N)$,

and moreover satisfies

- (ii) $\|\nu_z\|_{\mathcal{M}(\mathbb{R}^N)} \leq 1$ for a.e. $z \in D$;
 (iii) If $K \subset \mathbb{R}^N$ is closed and $\text{supp } \nu_z^n \subset K$ for a.e. $z \in D$ and n large, then $\text{supp } \nu_z \subset K$ for a.e. $z \in D$.

Suppose further that for every bounded, measurable $E \subset D$, there is a nonnegative $\kappa \in C(\mathbb{R}^N)$ with $\lim_{|\xi| \rightarrow \infty} \kappa(\xi) = \infty$ such that

$$\sup_n \int_E \langle \nu_z^n, \kappa \rangle dz < \infty. \quad (\text{A.1})$$

Then

(iv) $\|\nu_z\|_{\mathcal{M}(\mathbb{R}^N)} = 1$ for a.e. $z \in D$,

whence $\nu \in \mathbf{Y}(D, \mathbb{R}^N)$.

Proof. The proof is a generalization of Ball [4].

Denote by $L_w^\infty(D; \mathcal{M}(\mathbb{R}^N))$ the set of weak* measurable functions $\mu : D \rightarrow \mathcal{M}(\mathbb{R}^N)$, equipped with the norm

$$\|\mu\|_{\infty, \mathcal{M}} := \operatorname{ess\,sup}_{z \in D} \|\mu_z\|_{\mathcal{M}}.$$

From the fact that $C_0(\mathbb{R}^N)$ is separable it can be shown (e.g., [4]) that $L_w^\infty(D; \mathcal{M}(\mathbb{R}^N))$ is isometrically isomorphic to the dual of $L^1(D; C_0(\mathbb{R}^N))$. The sequence μ^n is bounded in $L_w^\infty(D; \mathcal{M}(\mathbb{R}^N))$ since $\|\mu^n\|_{\infty, \mathcal{M}} \equiv 1$, and hence there is a $\mu \in L_w^\infty(D; \mathcal{M}(\mathbb{R}^N))$ and a weak* convergent subsequence μ^m of μ^n such that $\langle \mu^m, \Psi \rangle_{\infty, \mathcal{M}} \rightarrow \langle \mu, \Psi \rangle_{\infty, \mathcal{M}}$, or equivalently,

$$\int_D \langle \mu_z^m, \Psi(z, \cdot) \rangle dz \rightarrow \int_D \langle \mu_z, \Psi(z, \cdot) \rangle dz \quad \text{as } m \rightarrow \infty$$

for all $\Psi \in L^1(D; C_0(\mathbb{R}^N))$. In particular, letting $\Psi(z, \xi) = \varphi(z)g(\xi)$ for $\varphi \in L^1(D)$ and $g \in C_0(\mathbb{R}^N)$, we obtain (iii). We claim that $\mu_z \geq 0$ for a.e. $z \in D$. If not, then there would be a nonnegative $\Psi \in L^1(D; C_0(\mathbb{R}^N))$ such that $\int_D \langle \mu_z, \Psi(z, \cdot) \rangle dz < 0$. But then

$$0 > \int_D \langle \mu_z, \Psi(z, \cdot) \rangle dz = \lim_{m \rightarrow \infty} \int_D \langle \mu_z^m, \Psi(z, \cdot) \rangle dz \geq 0$$

(since $\mu_z^m \geq 0$ for all z), a contradiction.

(i) follows from the weak* lower semicontinuity of the norm $\|\cdot\|_{\infty, \mathcal{M}}$. To see that (ii) holds, let $g \in C_0(\mathbb{R}^N)$ be such that $g|_K = 0$. Since $\mu^m \rightarrow K$ in measure, it follows that $\langle \mu^m, g \rangle \rightarrow 0$ in measure (that is, $|\{z \in D : |\langle \mu_z^m, g \rangle| > \delta\}| \rightarrow 0$ for all $\delta > 0$). Hence,

$$\int_D \varphi(z) \langle \mu_z, g \rangle dz = \lim_m \int_D \varphi(z) \langle \mu_z^m, g \rangle dz = 0$$

for all $\varphi \in L^1(D)$, and therefore $\langle \mu_z, g \rangle = 0$ for a.e. $z \in D$. This is precisely (ii).

Assume now that (A.1) holds. Fix a set $E \subset D$ of finite, nonzero Lebesgue measure $|E|$, and denote the average integral over E as $f_E = \frac{1}{|E|} \int_E$. For every $R > 0$ we define

$$\theta_R(\xi) = \begin{cases} 1 & \kappa(\xi) \leq R \\ 1 + R - \kappa(\xi) & R < \kappa(\xi) \leq R + 1 \\ 0 & R + 1 < \kappa(\xi). \end{cases}$$

Then $\theta_R \in C_0(\mathbb{R}^N)$, so

$$\lim_m \int_E \langle \mu_z^m, \theta_R \rangle dz = \int_E \langle \mu_z, \theta_R \rangle dz \leq \int_E \|\mu_z\|_{\mathbb{R}} dz \leq 1,$$

the last inequality following from the fact that $\|\mu_z\|_{\mathbb{R}} \leq 1$ for all z . Conversely,

$$0 \leq \int_E (1 - \langle \mu_z^m, \theta_R \rangle) dz = \int_E \langle \mu_z^m, 1 - \theta_R \rangle dz \leq \frac{1}{R} \int_E \langle \mu_z^m, \kappa \rangle dz,$$

so (A.1) gives

$$\begin{aligned} 1 &\leq \lim_{R \rightarrow \infty} \lim_m \int_E \langle \mu_z^m, \theta_R \rangle dz + \lim_{R \rightarrow \infty} \sup_m \frac{1}{R} \int_E \langle \mu_z^m, \kappa \rangle dz \\ &= \lim_{R \rightarrow \infty} \int_E \langle \mu_z, \theta_R \rangle dz \\ &\leq \int_E \|\mu_z\|_{\mathbb{R}} dz \leq 1, \end{aligned}$$

whence $\int_E \|\mu_z\|_{\mathbb{R}} dz = 1$. Since $E \subset D$ is arbitrary, (iv) follows. \square

A.2.6 An important special case of (A.1) is when $\kappa(\xi) = |\xi|^p$ for $1 \leq p < \infty$, which translates to the L^p bound

$$\sup_n \int_D \langle \mu^n, |\xi|^p \rangle dz < \infty.$$

The case $p = \infty$ translates to the support of ν_z^n lying in a compact set $K \subset \mathbb{R}^N$ for a.e. z and all n . Part (iii) of Theorem A.1 then holds for all $g \in C(\mathbb{R}^N)$, and condition (A.1) is automatically satisfied for any such κ . The latter is the original form of the theorem given by Tartar [62].

A.3 Random fields and Young measures

A.3.1 If (Ω, \mathcal{F}, P) is a probability space, $D \subset \mathbb{R}^k$ is a Borel set and $u : \Omega \times D \rightarrow \mathbb{R}^N$ is a random field (i.e., a jointly measurable function), then we can define its law by

$$\nu_z(F) := P(u(z) \in F) = P(\{\omega : u(\omega, z) \in F\}) \quad (\text{A.2a})$$

for Borel subsets $F \subset \mathbb{R}^N$ of phase space, or equivalently,

$$\langle \nu_z, g \rangle := \int_{\Omega} g(u(\omega, z)) dP(\omega) \quad (\text{A.2b})$$

for $g \in C_0(\mathbb{R}^N)$. This defines a Young measure:

Proposition A.2. If $u : \Omega \times D \rightarrow \mathbb{R}^N$ is jointly measurable then (A.2) defines a Young measure from D to \mathbb{R}^N .

Proof. First of all, for fixed $z \in D$ the set $\{\omega : u(\omega, z) \in U\}$ is P -measurable for Borel sets U . Indeed, if $w(\omega) := u(\omega, z)$ denotes the z -section of the measurable function $(\omega, y) \mapsto u(\omega, y)$, then $\{\omega : u(\omega, z) \in U\} = w^{-1}(U)$ is measurable.

We need to show that the definition of ν is independent of the choice of mapping in the equivalence classes of mappings from $\Omega \times D \rightarrow \mathbb{R}^N$. Let $\hat{u}, \tilde{u} : \Omega \times D \rightarrow \mathbb{R}^N$ be two mappings such that $\hat{u}(\omega, z) = \tilde{u}(\omega, z)$ for $P \times \lambda$ -a.e. (ω, z) . We apply Tonelli's theorem to find that

$$0 = \int_{\Omega \times D} \mathbb{1}_{\{\hat{u} \neq \tilde{u}\}}(\omega, z) d(P \times \lambda)(\omega, z) = \int_D P(\{\hat{u}(z) \neq \tilde{u}(z)\}) dz.$$

Hence, $P(\hat{u}(z) \neq \tilde{u}(z)) = 0$ for a.e. $z \in D$, so for every Borel set $U \subset \mathbb{R}^N$,

$$P(\hat{u}(z) \in U) = P(\tilde{u}(z) \in U)$$

for a.e. $z \in D$.

Finally, ν is weak* measurable since

$$\langle \nu_z, g \rangle = \int_{\mathbb{R}^N} g(\xi) d\nu_z(\xi) = \int_{\Omega} g(u(\omega, z)) dP(\omega),$$

which is measurable in z for any $g \in C_0(\mathbb{R}^N)$. □

A.3.2 It is well known that every measure on \mathbb{R}^N can be realized as the law of a random variable. Here we show that for every Young measure ν , there is always a random variable with law ν . The novelty here is that the random variable $u = u(\omega, z)$ is measurable in (ω, z) .

Proposition A.3. For every Young measure $\nu \in \mathbf{Y}(D, \mathbb{R}^N)$ there exists a probability space (Ω, \mathcal{F}, P) and a function $u : \Omega \times D \rightarrow \mathbb{R}^N$ such that

- u is measurable on the product σ -algebra on $\Omega \times D$
- u has law ν , i.e. for all Borel sets E ,

$$\nu_z(E) = P(u(\omega, z) \in E).$$

In particular, we can choose (Ω, \mathcal{F}, P) to be the Borel σ -algebra on $\Omega = [0, 1)$ with Lebesgue measure.

Proof. The method of proof is standard; see e.g. [7, Theorem 5.3].

We assume that $N = 1$. The generalization to $N > 1$ is straightforward but tedious. For $n \in \mathbb{N}$ and $j \in \mathbb{Z}$, we set

$$F_n^j := \begin{cases} (-\infty, -2^n) & \text{if } j = -2^{2n} \\ [2^{-n}(j-1), 2^{-n}j) & \text{if } j = -2^{2n} + 1, \dots, 2^{2n} \\ [2^n, \infty) & \text{if } j = 2^{2n} + 1 \\ \emptyset & \text{otherwise.} \end{cases}$$

Let $p_n^j(z) := \sum_{l \leq j} \nu_z(F_n^l)$. Note that $p_n^j : \mathbb{R} \rightarrow [0, 1]$ is measurable for all n, j , and that $p_n^{-j} = 0$ and $p_n^j = 1$ for large j . Choose any $\xi_n^j \in F_n^j$, and for $\omega \in \Omega := [0, 1)$, define

$$u_n(\omega, z) := \xi_n^j \quad \text{for } j \text{ such that } p_n^{j-1}(z) \leq \omega < p_n^j.$$

We claim that u_n is measurable on the product σ -algebra between \mathcal{F} and the Borel σ -algebra on D . Each function u_n takes only finitely many values ξ_n^j , so it suffices to show that $u_n^{-1}(\{\xi_n^j\})$ is measurable for every ξ_n^j . Indeed,

$$\begin{aligned} u_n^{-1}(\{\xi_n^j\}) &= \left\{ (\omega, z) \in \Omega \times D : p_n^j(z) \leq \omega < p_n^{j+1}(z) \right\} \\ &= \left(\Omega \times D \right) \cap \left\{ (\omega, z) \in \mathbb{R} \times D : p_n^j(z) \leq \omega \right\} \cap \left\{ (\omega, z) \in \mathbb{R} \times D : \omega < p_n^{j+1}(z) \right\}, \end{aligned}$$

the intersection between the epigraph of p_n^j and the hypograph of p_n^{j+1} , which are measurable by the measurability of the functions p_n^j and p_n^{j+1} .

Because the partition $\{F_m^j\}_{j \in \mathbb{Z}}$ is a refinement of $\{F_n^j\}_{j \in \mathbb{Z}}$ whenever $m > n$, it follows that $|u_n(\omega, z) - u_m(\omega, z)| < \text{diam}(F_n^j) = 2^{-n}$ for any (ω, z) whenever m, n are large enough. Hence, u_n converges pointwise to some function $u : \Omega \times D \rightarrow \mathbb{R}$, which is measurable by the measurability of each u_n .

Finally, for every $g \in C_0(\mathbb{R})$ and $z \in D$, we have by Lebesgue's dominated convergence theorem

$$\int_{\Omega} g(u(\omega, z)) dP(\omega) = \lim_n \int_{\Omega} g(u_n(\omega, z)) dP(\omega) = \lim_n \sum_j \nu_z(F_n^j) g(\xi_n^j) = \int_{\mathbb{R}} g(\xi) d\nu_z(\xi).$$

Hence, $u(\cdot, z)$ has law ν_z . □

B Proof of Theorem 4.9

Proof. For any random field $\zeta : \Omega \rightarrow L^1(\mathbb{R}^d \times \mathbb{R}_+) \cap L^\infty(\mathbb{R}^d \times \mathbb{R}_+)$ on (Ω, \mathcal{F}, P) , we denote the expectation with respect to the probability measure P as

$$\mathbb{E}(\zeta) := \int_{\Omega} \zeta(\omega) dP(\omega).$$

For $1 \leq k \leq M$, denote

$$\begin{aligned} G(\omega) &= \int_{\mathbb{R}_+} \int_{\mathbb{R}^d} \psi(x, t) g(u^{\Delta x}(\omega; x, t)) dx dt, \\ G_k(\omega) &= \int_{\mathbb{R}_+} \int_{\mathbb{R}^d} \psi(x, t) g(u^{\Delta x, k}(\omega; x, t)) dx dt. \end{aligned} \tag{B.1}$$

Henceforth we suppress the ω -dependence of G and G_k for notational convenience. The $L^2(P)$ error in the approximation can be written as

$$\begin{aligned}
\mathbb{E} \left(\left(\mathbb{E}(G) - \frac{1}{M} \sum_{k=1}^M G_k \right)^2 \right) &= \mathbb{E} \left(\frac{1}{M^2} \left(\sum_{k=1}^M (\mathbb{E}(G) - G_k) \right)^2 \right), \\
&= \mathbb{E} \left(\frac{1}{M^2} \left(\sum_{k=1}^M (\mathbb{E}(G) - G_k)^2 + 2 \sum_{k=1}^M \sum_{l \neq k} (\mathbb{E}(G) - G_k)(\mathbb{E}(G) - G_l) \right) \right) \\
&= \underbrace{\frac{1}{M^2} \sum_{k=1}^M \mathbb{E} \left((\mathbb{E}(G) - G_k)^2 \right)}_{=: T_1} + \frac{2}{M^2} \sum_{k=1}^M \sum_{l \neq k} \underbrace{\mathbb{E} \left((\mathbb{E}(G) - G_k)(\mathbb{E}(G) - G_l) \right)}_{=: T_2^{kl}}.
\end{aligned}$$

As $u^{\Delta x, 1}, \dots, u^{\Delta x, M}$ are independent and identically distributed, it follows from the definition of G_k that G_1, \dots, G_M are independent and identically distributed random variables. Hence, $\mathbb{E}(G_k) = \mathbb{E}(G)$ and $\mathbb{E}(G_k G_l) = \mathbb{E}(G_k)\mathbb{E}(G_l)$ for all k, l . Consequently, a simple calculation shows that $T_2^{kl} = 0$ for all $1 \leq k, l \leq M$ and $k \neq l$.

The fact that G_1, \dots, G_M are independent and identically distributed yields

$$T_1 = \frac{1}{M} (\mathbb{E}(G^2) - (\mathbb{E}(G))^2).$$

Hence,

$$\begin{aligned}
\mathbb{E} \left(\left(\mathbb{E}(G) - \frac{1}{M} \sum_{k=1}^M G_k \right)^2 \right) &= \frac{1}{M} (\mathbb{E}(G^2) - (\mathbb{E}(G))^2) \\
&\leq \frac{1}{M} \|g(u^{\Delta x})\|_{L^\infty(\Omega \times \mathbb{R}^d \times \mathbb{R}_+)}^2 \|\psi\|_{L^1(\mathbb{R}^d \times \mathbb{R}_+)}^2 \quad (\text{by definition (B.1)}) \\
&\leq \frac{C}{M} \quad (\text{by assumption (4.3a)}).
\end{aligned}$$

In conclusion, the sample mean

$$\frac{1}{M} \sum_{k=1}^M \int_{\mathbb{R}_+} \int_{\mathbb{R}^d} \psi(x, t) g(u^{\Delta x, k}(x, t)) \, dx dt$$

converges to the corresponding ensemble average

$$\int_{\mathbb{R}_+} \int_{\mathbb{R}^d} \psi(x, t) \langle \nu_{x, t}^{\Delta x}, g \rangle \, dx dt$$

in $L^2(\Omega; P)$ with a convergence rate of $\frac{1}{\sqrt{M}}$. Taking a subsequence $M' \rightarrow \infty$, the convergence also holds P -almost surely. \square

C Time continuity of approximations

From the time integration procedure (4.1b) we can show that the approximate MV solutions are time continuous. Consequently, the initial data is attained in a certain sense, and moreover, it is meaningful to evaluate the MV solution at a specific time t .

We state the theorem without proof, since the results are straightforward generalizations of “deterministic” counterparts.

Theorem C.1. Let $\psi \in C_c^1(\mathbb{R})$ and assume that (4.3a) and (4.3b) are satisfied. Let $\nu^{\Delta x}$ be generated by Algorithm 4.1. Then the functions

$$\Psi^{\Delta x}(t) := \int_{\mathbb{R}} \psi(x) \langle \nu_{(x,t)}^{\Delta x}, \text{id} \rangle dx$$

and

$$\Psi(t) := \int_{\mathbb{R}} \psi(x) \langle \nu_{(x,t)}, \text{id} \rangle dx$$

are Hölder continuous with exponent $\gamma := \frac{r-1}{r}$ and with constant independent of Δx , and $\Psi^{\Delta x}(t) \rightarrow \Psi(t)$ as $\Delta x \rightarrow 0$ for a.e. $t \in [0, T]$. Moreover,

$$\Psi(0) = \lim_{t \rightarrow 0} \Psi(t) = \int_{\mathbb{R}} \psi(x) \langle \sigma_x, \text{id} \rangle dx.$$

References

- [1] L. Ambrosio, N. Gigli and G. Savaré. Gradient Flows. Birkhäuser Basel, 2005.
- [2] E. J. Balder. New Fundamentals of Young Measure Convergence. Calculus of Variations and Optimal Control, in CRC Research Notes in Mathematics 410, A. Ioffe, S. Reich and I. Shafirir eds, 1999.
- [3] E. J. Balder. Lectures on Young Measures. Université de Paris-Dauphine, 1995.
- [4] J. Ball. A version of the fundamental theorem for Young measures. In PDEs and Continuum Models of Phase Transitions (M. Rascle, D. Serre and M. Slemrod, eds.), Lecture Notes in Physics, vol. 344, Springer, 1989. 207–215.
- [5] T. J. Barth. Numerical methods for gas-dynamics systems on unstructured meshes. In An Introduction to Recent Developments in Theory and Numerics of Conservation Laws, Lecture Notes in Computational Science and Engineering volume 5, Springer, Berlin. Eds: D. Kroner, M. Ohlberger, and Rohde, C., 1999, 195–285.
- [6] S. Bianchini and A. Bressan. Vanishing viscosity solutions of nonlinear hyperbolic systems. Ann. of Math. (2) 161 (2005), no. 1, 223–342.
- [7] P. Billingsley. Probability and Measure 3rd ed. John Wiley & Sons Inc., 1995.
- [8] P. Billingsley. Convergence of Probability Measures. John Wiley & Sons, Inc, 2008.

- [9] Y. Brenier and C. De Lellis and L. Székelyhidi Jr. Weak-Strong Uniqueness for Measure-Valued Solutions. *Comm. Math. Phys.*, 305 (2), 2011, 351–361.
- [10] A. Bressan, G. Crasta and B. Piccoli. Well-posedness of the Cauchy problem for $n \times n$ systems of conservation laws. *Memoirs of the AMS*, 146 (694), 2000.
- [11] Central Station: high-resolution non-oscillatory central schemes for non-linear conservation laws and related problems, www.cscamm.umd.edu/centpack/publications/
- [12] G. Q. Chen and J. Glimm. Kolmogorov’s theory of turbulence and inviscid limit of the Navier-Stokes equations in \mathbb{R}^3 . *Comm. Math. Phys.* 310 (1), 2012, 267–283.
- [13] B. Cockburn, F. Coquel and P. G. LeFloch. Convergence of the finite volume method for multidimensional conservation laws. *SIAM J. Numer. Anal.*, 32 (3), 1995, 687–705.
- [14] B. Cockburn, C. Johnson, C. -W. Shu and E. Tadmor. *Advanced Numerical Approximation of Nonlinear Hyperbolic Equations*. Lecture notes in Mathematics 1697, 1997 C.I.M.E. course in Cetraro, Italy, June 1997 (A. Quarteroni ed.), Springer Verlag 1998.
- [15] B. Cockburn and C-W. Shu. TVB Runge-Kutta local projection discontinuous Galerkin finite element method for conservation laws. II. General framework. *Math. Comput.*, 52, 1989, 411–435.
- [16] M. G. Crandall and A. Majda. Monotone difference approximations for scalar conservation laws. *Math. Comput.* 34, 1980, 1–21.
- [17] C. Dafermos. *Hyperbolic conservation laws in continuum physics*. Springer, Berlin, 2000.
- [18] C. De Lellis, L. Székelyhidi Jr. The Euler equations as a differential inclusion. *Ann. of Math.* (2) 170 (2009), no. 3, 1417–1436.
- [19] E. Chiodaroli, C. De Lellis, O. Kreml. Global ill-posedness of the isentropic system of gas dynamics. Preprint, 2013.
- [20] S. Demoulini and D. M. A. Stuart and A. E. Tzavaras. Weak-strong uniqueness of dissipative measure-valued solutions for polyconvex elastodynamics. *Archives of Rational Mechanics and Analysis*, 205 (3), 2012, 927–961.
- [21] B. Depres, G. Poette and D. Lucor. Uncertainty quantification for systems of conservation laws. *J. Comput. Phys.* 228 (2009), no. 7, 2443–2467.
- [22] R. J. DiPerna. Measure valued solutions to conservation laws. *Arch. Rational Mech. Anal.*, 88(3), 1985, 223–270.
- [23] R. J. DiPerna and A. Majda. Oscillations and concentrations in weak solutions of the incompressible fluid equations. *Comm. Math. Phys.* 108 (4), 1987, 667–689.
- [24] U. S. Fjordholm, S. Mishra and E. Tadmor. ENO reconstruction and ENO interpolation are stable. *FoCM* 13 (2), 2013, 139–159.

- [25] U. S. Fjordholm, S. Mishra and E. Tadmor. Arbitrary order accurate essentially non-oscillatory entropy stable schemes for systems of conservation laws. *SIAM J. Num. Anal* 50 (2), 2012, 544–573.
- [26] U. S. Fjordholm. High-order accurate entropy stable numerical schemes for hyperbolic conservation laws. ETH Zürich dissertation Nr. 21025, 2013.
- [27] U. S. Fjordholm and S. Mishra. Convergence of entropy stable finite difference schemes to measure valued solutions of hyperbolic systems of conservation laws. In preparation, 2013.
- [28] G. B. Folland. *Real Analysis*. John Wiley & Sons Inc, 1999.
- [29] F. Fuchs, A. McMurry, S. Mishra, N. H. Risebro and K. Waagan. Approximate Riemann solver based high-order finite volume schemes for the MHD equations in multi-dimensions. *Comm. Comput. Phys* 9, 2011, 324–362.
- [30] H. Frid and I-S. Liu. Oscillation waves in Riemann problems for phase transitions. *Quart. Appl. Math.* 56 (1), 1998, 115–135.
- [31] H. Frid and I-S. Liu. Oscillation waves in Riemann problems inside elliptic regions for conservation laws of mixed type. *Z. Angew. Math. Phys.* 46 (1995), no. 6, 913–931.
- [32] S. Gottlieb, C.-W. Shu and E. Tadmor. High order time discretizations with strong stability properties. *SIAM. Review* 43, 2001, 89–112.
- [33] J. Glimm. Solutions in the large for nonlinear hyperbolic systems of equations. *Comm. Pure Appl. Math.* 18 (4), 1965, 697-715.
- [34] J. Glimm, J. Grove and Y. Zhang, Numerical Calculation of Rayleigh-Taylor and Richtmyer-Meshkov Instabilities for Three Dimensional Axisymmetric flows in Cylindrical and Spherical Geometries. Los Alamos Laboratory, Report# LA-UR99-6796, 1999.
- [35] Edwige Godlewski and Pierre A. Raviart. *Hyperbolic Systems of Conservation Laws. Mathematiques et Applications, Ellipses Publ., Paris (1991)*.
- [36] A. Harten. High resolution schemes for hyperbolic conservation laws *J. Comput. Phys.* 49, 1983, 357–393.
- [37] A. Harten, B. Engquist, S. Osher and S. R. Chakravarty. Uniformly high order accurate essentially non-oscillatory schemes, III. *J. Comput. Phys.* 71 (2), 1987, 231–303.
- [38] A. Hildebrand and S. Mishra. Entropy stable shock capturing streamline diffusion space-time discontinuous Galerkin (DG) methods for systems of conservation laws. *Num. Math.*, to appear, 2013.
- [39] J. Jaffre, C. Johnson and A. Szepessy. Convergence of the discontinuous Galerkin finite element method for hyperbolic conservation laws. *Math. Model. Meth. Appl. Sci.*, 5(3), 1995, 367–386.

- [40] G.-S. Jiang and C.-W. Shu. Efficient implementation of weighted ENO schemes. *J. Comput. Phys.*, 126(1), 1996, 202–228.
- [41] C. Johnson and A. Szepessy. On the convergence of a finite element method for a nonlinear hyperbolic conservation law. *Math. Comput.*, 49 (180), 1987, 427–444.
- [42] R. Käppeli. Numerical methods for 3D magneto-rotational core-collapse supernova simulation with jet formation. Ph.D thesis, University of Basel, 2011.
- [43] S. N. Kruzhkov. first order quasilinear equations in several independent variables. *USSR Math. Sbornik.*, 10 (2), 1970, 217–243.
- [44] N.N. Kuznetsov. Accuracy of some approximate methods for computing the weak solutions of a first-order quasi-linear equation. *USSR Comput. Math. and Math. Phys.* 16 (1976), 105–119.
- [45] P. D. Lax. Hyperbolic systems of conservation laws II. *Comm. Pure Appl. Math.* 10 (4), 1957, 537-566.
- [46] P. D. Lax. Mathematics and Physics. *Bull. AMS* 45(1), 2007, 135-152.
- [47] P. G. LeFloch, J. M. Mercier and C. Rohde. Fully discrete entropy conservative schemes of arbitrary order. *SIAM J. Numer. Anal.*, 40 (5), 2002, 1968–1992.
- [48] R. J. LeVeque. Finite volume methods for hyperbolic problems. Cambridge university press, Cambridge, 2002.
- [49] H. Lim, Y. Yu, J. Glimm, X. L. Li and D. H. Sharp. Chaos, transport and mesh convergence for fluid mixing. *Act. Math. Appl. Sin.*, 24 (3), 2008, 355–368.
- [50] P. Major. On the invariance principle for sums of independent identically distributed random variables. *Journal of Multivariate Analysis* 8 (4), 1978, 487–517.
- [51] S. Mishra and C. Schwab. Sparse tensor multi-level Monte Carlo finite volume methods for hyperbolic conservation laws with random initial data. *Math. Comput.*, 81(180), 2012, 1979–2018.
- [52] S. Mishra, Ch. Schwab and J. Sukys. Multi-level Monte Carlo finite volume methods for nonlinear systems of conservation laws in multi-dimensions. *J. Comput. Phys* 231 (8), 2012, 3365–3388.
- [53] S. Mishra, Ch. Schwab and J. Sukys. Monte Carlo and multi-level Monte Carlo finite volume methods for uncertainty quantification in nonlinear systems of balance laws. *Uncertainty Quantification in Computational Fluid Dynamics. Lecture Notes in Computational Science and Engineering* Volume 92, 2013, 225–294
- [54] S. Mishra, N.H. Risebro, Ch. Schwab and S. Tokareva. Numerical solution of scalar conservation laws with random flux functions. Research report 2012-35, SAM ETH Zürich.

- [55] J. Munkres. Algorithms for the Assignment and Transportation Problems *Journal of the Society for Industrial and Applied Mathematics*, 5 (1), 1957, 32–38.
- [56] B. Perthame and E. Tadmor. A kinetic equation with kinetic entropy functions for scalar conservation laws. *Communications in Mathematical Physics* 136, 1991, 501-517.
- [57] S. Schochet. Examples of measure-valued solutions *Comm. Par. Diff. Eqns.* 14 (5), 1989, 545–575.
- [58] M. Schonbeck. Convergence of solutions to nonlinear dispersion equations. *Comm. Par. Diff. Eqns.* 7 (8), 1982, 959–1000.
- [59] E. Tadmor. The numerical viscosity of entropy stable schemes for systems of conservation laws, I. *Math. Comp.* 49, 1987, 91–103.
- [60] E. Tadmor. Entropy stability theory for difference approximations of nonlinear conservation laws and related time-dependent problems. *Act. Numerica.*, 2003, 451-512.
- [61] E. Tadmor. Convergence of spectral methods for nonlinear conservation laws. *SIAM Journal on Numerical Analysis* 26 (1989), 30–44.
- [62] L. Tartar. Compensated compactness and applications to partial differential equations. *Nonlinear analysis and mechanics: Heriot-Watt Symposium, Vol. IV, Pitman*, 1979, 136–212.